IMMUNOLOGY

The immune checkpoint B7-H3 (CD276) regulates adipocyte progenitor metabolism and obesity development

Elodie Picarda[1]†, Phillip M. Galbo Jr.[1,2], Haihong Zong[3], Meenu Rohini Rajan[4], Ville Wallenius[5], Deyou Zheng[2,6], Emma Börgeson[4,7], Rajat Singh[3,8], Jeffrey Pessin[3,8], Xingxing Zang[1,3,8]*

The immune checkpoint B7-H3 (CD276) is a member of the B7 family that has been studied in the tumor microenvironment and immunotherapy, but its potential role in metabolism remains largely unknown. Here, we show that B7-H3 is highly expressed in mouse and human adipose tissue at steady state, with the highest levels in adipocyte progenitor cells. B7-H3 is rapidly down-regulated upon the initiation of adipocyte differentiation. Combined RNA sequencing and metabolic studies reveal that B7-H3 stimulates glycolytic and mitochondrial activity of adipocyte progenitors. Loss of B7-H3 in progenitors results in impaired oxidative metabolism program and increased lipid accumulation in derived adipocytes. Consistent with these observations, mice knocked out for B7-H3 develop spontaneous obesity, metabolic dysfunction, and adipose tissue inflammation. Our results reveal an unexpected metabolic role for B7-H3 in adipose tissue and open potential new avenues for the treatment of metabolic diseases by targeting the B7-H3 pathway.

INTRODUCTION

The interactions between members of the B7 ligand family with their corresponding receptors in the CD28 family provide signals of costimulation and coinhibition to lymphocytes to regulate immune responses (*1*). B7-H3 (CD276), a member of the B7 family, is a type I transmembrane protein composed of one pair of immunoglobulin V (IgV) and IgC ectodomains in mice and two IgV-IgC domains repeated in tandem in humans. Basal B7-H3 protein expression is low and restricted only to certain cell types including fibroblasts, progenitors, and immune cells. Notably, B7-H3 is overexpressed in the vast majority of human cancers and correlates with poor clinical outcome (*2*). It exerts multiple functions from the regulation of innate and adaptive immunity to the control of bone formation and tumor growth. The B7-H3 pathway has remained elusive because no potential ligands or receptors have been described so far. Two recent studies showed that B7-H3 controls aerobic glycolysis in cancer cells, either by reactive oxygen species (ROS)–mediated stabilization of hypoxia-inducible factor 1α (HIF1α) (*3*) or by regulating hexokinase 2 (HK2) (*4*), suggesting its association with metabolic signaling. This pathological role exhibited by B7-H3 during malignancy indicates that this protein might also harbor physiological functions in healthy tissues.

Obesity has become an epidemic in developed countries across the world. In 2017–2018, the prevalence of obesity was 42.4% in the United States (*5*). Worldwide obesity has nearly tripled since 1975, with a total of 650 million obese adults in 2016 (World Health Organization; www.who.int/news-room/fact-sheets/detail/obesity-and-overweight). Obesity causes adipocyte dysregulation and the release of proinflammatory cytokines and adipokines that, in turn, recruit proinflammatory immune cells into the fat tissue. Inflammatory cells worsen insulin resistance, thus enhancing adipose tissue dysfunction. This ultimately results in metabolic syndrome, a serious condition that significantly increases the risk for developing type 2 diabetes, cardiovascular diseases, hepatic steatosis, periodontal disease, and a number of cancers. Although classically associated with Western diet habit, obesity is also linked to certain genetic factors causing deregulation of glucose and lipid metabolism, adipogenesis, and insulin signaling (*6*–*9*). Individuals harboring such genetic disruptions or polymorphisms can become overweight even with low-calorie diets, suggesting that obesity can be induced not only by excess nutrient intake but also by deregulations per se in energy storage and utilization by the adipose tissue. The intricate pathways by which adipocytes control their metabolism, lipid fate, and how these connect to adipose dysfunction and inflammation remain poorly understood.

Here, we show that the immune checkpoint B7-H3 is abundantly expressed in mouse and human adipose tissues, with preferential expression in adipocyte progenitors (APs). Lack of B7-H3 in APs alters their transcriptional program characterized by changes in carbohydrate metabolism and oxidative phosphorylation. Adipocytes derived from B7-H3–null progenitors exhibit impaired mitochondrial function and increased lipid storage. Consequently, mice knocked out for B7-H3 develop spontaneous obesity, which associates with loss of metabolic and immune homeostasis. Thus, the immune checkpoint B7-H3 is an intrinsic pathway that regulates APs and adipocyte metabolism and fat tissue homeostasis.

RESULTS

B7-H3 is highly expressed in adipose tissue and is dysregulated with obesity

As the role of B7-H3 has largely been studied in tumors and inflamed tissues, we asked whether B7-H3 also controls cell function

[1]Department of Microbiology and Immunology, Albert Einstein College of Medicine, Bronx, NY 10461, USA. [2]Department of Genetics, Albert Einstein College of Medicine, Bronx, NY 10461, USA. [3]Department of Medicine, Albert Einstein College of Medicine, Bronx, NY 10461, USA. [4]Institute of Medicine, Department of Molecular and Clinical Medicine, The Wallenberg Laboratory and Wallenberg Centre for Molecular and Translational Medicine, University of Gothenburg, Gothenburg, Sweden. [5]Department of Gastrosurgical Research and Education, Institute of Clinical Sciences, Sahlgrenska Academy, University of Gothenburg, Gothenburg, Sweden. [6]Departments of Neurology and Neuroscience, Albert Einstein College of Medicine, Bronx, NY 10461, USA. [7]Department of Clinical Physiology, Region Vaestra Goetaland, Sahlgrenska University Hospital, Gothenburg, Sweden. [8]Einstein-Mount Sinai Diabetes Research Center, Albert Einstein College of Medicine, Bronx, NY 10461, USA.
*Corresponding author. Email: xingxing.zang@einsteinmed.org
†Present address: Regeneron Pharmaceuticals, 777 Old Saw Mill River Rd, Tarrytown, NY 10591, USA.

under normal physiologic states. To this purpose, we first analyzed B7-H3 expression levels at steady state across 54 human tissues and 7 hematologic cells using RNA sequencing (RNA-seq) datasets from the Genotype-Tissue Expression (GTEx), FANTOM5, and Human Protein Atlas (HPA) project (www.proteinatlas.org/ENSG00000103855-CD276/tissue). Combining all three sources showed that *B7-H3* expression was highest in adipose tissue and lowest in hematologic cells (Fig. 1A). These results suggest an important homeostatic function for B7-H3 in adipose tissue. Next, we studied the correlation between *B7-H3* gene expression and obesity across multiple human cohorts. In the METSIM (METabolic Syndrome In Men) study (cohort 1) (*10*), RNA was obtained from subcutaneous fat biopsies from randomly selected 770 Finnish men with a wide range of body weight and insulin sensitivity. Our analyses of this dataset revealed that *B7-H3* gene expression was positively correlated with body mass index (BMI) (Fig. 1B) and percent fat mass (Fig. 1C) but negatively associated with the Matsuda index (Fig. 1D), a universally accepted measure of insulin sensitivity. In our analyses of a second

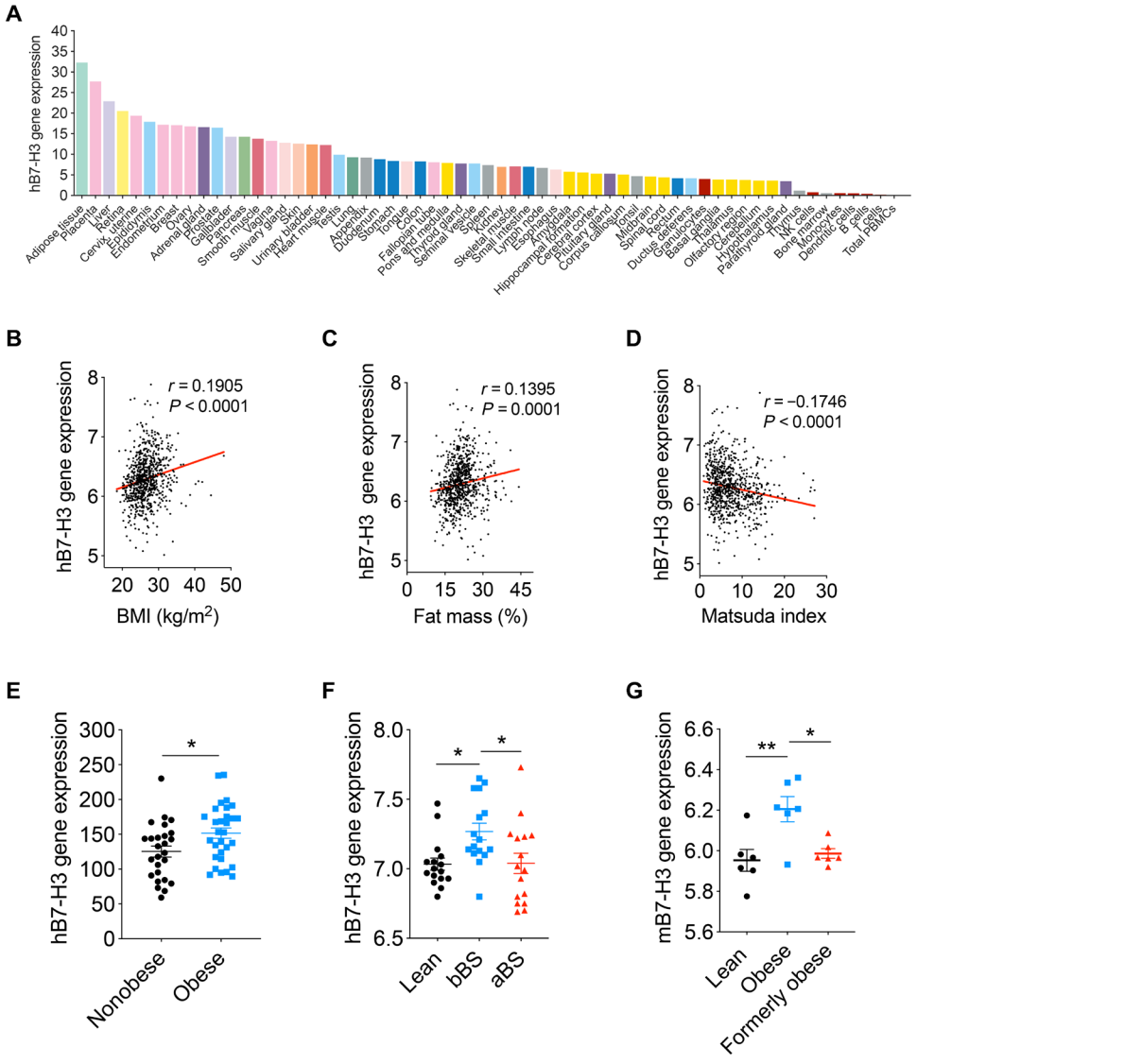

Fig. 1. B7-H3 is highly expressed in adipose tissue and dysregulated with obesity. (**A**) Normalized consensus human B7-H3 (hB7-H3) RNA expression across human tissues and blood cells by combining the data from the three transcriptomics datasets (HPA, GTEx, and FANTOM5) on the HPA. (**B** to **D**) Microarray analysis of hB7-H3 expression in subcutaneous fat biopsies of 770 men [GSE70353, METSIM study (*10*)] and correlation with BMI (B), percent of fat mass (C), and Matsuda index of insulin sensitivity (D). Red line represents nonlinear regression analysis with straight line fitting. *r*, correlation coefficient. (**E**) Microarray analysis of hB7-H3 gene expression in subcutaneous fat from lean nonobese ($n = 26$) and obese women ($n = 30$) [GSE25401 (*11*)]. (**F**) Microarray analysis of hB7-H3 in subcutaneous fat from obese women before (bBS, $n = 16$) and after (aBS, $n = 16$) bariatric surgery and from never-obese lean individuals (lean, $n = 16$) [GSE59034 (*12*)]. (**G**) Microarray analysis of mouse B7-H3 (mB7-H3) gene expression in gWAT from lean mice ($n = 6$), obese ($n = 6$), and formerly male obese mice ($n = 6$) [GSE97271 (*13*)]. Mice of the obese group received a high-fat high-sucrose diet (Research Diets, D12331; 58% kcal from fat) for 27 weeks, while mice of the lean group were given the low-fat control diet (Research Diets, D12329, 10.5% kcal from fat). After 20 weeks of feeding, a group of HFD-fed mice was switched to the low fat–containing control diet for another 7 weeks. Data are represented as means ± SEM in (E) to (G). Data were analyzed by Pearson correlation (B to D), Student's *t* test (E), and one-way analysis of variance (ANOVA) (F and G). $^*P < 0.05$ and $^{**}P < 0.01$.

cohort (*11*), we observed that obese women displayed higher adipose tissue expression of *B7-H3* than nonobese women (Fig. 1E). Last, our analyses of a third cohort of 16 women undergoing bariatric surgery (*12*) revealed the down-regulation of *B7-H3* expression after surgery to levels observed in lean controls who had no past history of obesity (Fig. 1F). On this premise, we analyzed the expression of *B7-H3* in datasets published from mouse studies. In a mouse dataset (*13*), we found that B7-H3 expression in white adipose tissue (WAT) was significantly up-regulated in wild-type (WT) mice fed with a high-fat diet (HFD) compared to a regular chow (Fig. 1G). Reverting obese mice to low-fat feeding for 7 weeks led to down-regulation of B7-H3 expression to levels observed in lean mice (Fig. 1G). Collectively, our analyses show that B7-H3 is highly expressed in adipose tissue at steady state and positively correlates with obesity in human and mice. Our analyses point to potential roles of B7-H3 in pathophysiology of obesity and metabolic disease.

B7-H3 is constitutively expressed in APs in mice and humans

Because B7-H3 is highly expressed in adipose tissue, we thought to identify which fat depot(s) and cell type(s) express B7-H3. First, we compared *B7-H3* gene expression in mouse white and brown fat. We found that B7-H3 mRNA was abundantly expressed in gonadal WAT (gWAT) and inguinal WAT (iWAT), while only modest expression was detected in brown adipose tissue (BAT) (Fig. 2A). The adipose tissue is a complex endocrine tissue composed of mature adipocytes along with stem AP, endothelial, and immune cells (*14*), collectively called the stromal vascular fraction (SVF). To identify which cell type(s) express B7-H3, mouse gWAT was dissociated into separate adipocytes and SVF for analysis of gene expression. *B7-H3* mRNA was highly expressed in the SVF as compared to primary adipocytes (Fig. 2B). Our analyses of a published mouse microarray dataset showed that the same is true for iWAT (fig. S1A) (*15*). We further confirmed that B7-H3 protein was expressed in mouse SVF cell lysate and absent in adipocytes by Western blotting as depicted in Fig. 2C. In contrast, perilipin, a lipid droplet–associated protein, was present in adipocytes but not detected in the SVF (Fig. 2C). These results suggest that B7-H3 is not expressed in primary adipocytes but is present in the fraction harboring their precursors. Consequently, we used flow cytometry to identify the expression of B7-H3 in a cell-specific manner, and we observed little to no expression of B7-H3 in $CD45^+$ immune cells and $CD31^+$ endothelial cells (Fig. 2, D and E). By contrast, B7-H3 was expressed in about 60% of the lineage-negative $CD45^-CD31^-Lin^-$ cells of the mouse SVF. These Lin^- cells contain several mesenchymal stromal cell populations of stem or progenitor type. Consequently, we analyzed the coexpression of B7-H3 with various markers of APs. B7-$H3^+$ cells highly coexpressed CD29, Sca1, and platelet-derived growth factor receptor α (PDGFRα) and, to a lesser extent, CD90 and CD34 (Fig. 2F and fig. S1B). In contrast, B7-$H3^-$ cells displayed low to intermediate levels of CD90, PDGFRα, and Sca1 (Fig. 2F). We further noted that more than 90% of $Lin^-CD29^+Sca1^+PDGFR\alpha^+$ cells, often referred to as APs (*16*) or adipose mesenchymal stromal cells, were positive for B7-H3 (Fig. 2G), suggesting that B7-H3 is a possible marker for this cell population.

Given our findings in mice, we then sought to assess the expression of B7-H3 in human adipose tissue. To this end, we analyzed microarray expression data of subcutaneous fat biopsies from the previously described METSIM cohort (*10*). We also analyzed microarray data from a separate cohort of nonobese individuals (*17*), wherein SVF and adipocytes were isolated from subcutaneous adipose tissue. Consistent with our results in mice, we found that B7-H3 expression negatively correlated with the *CD45* immune cell marker (Fig. 2H) and with adipocyte markers, adiponectin and perilipin (Fig. 2I and fig. S1C). By contrast, B7-H3 expression was found to predominantly enrich in the SVF (Fig. 2J) and associated positively with human adipose mesenchymal stem cells markers, *CD90*, *CD105*, and *CD73* (Fig. 2K). Furthermore, we analyzed B7-H3 expression in single-cell RNA-seq data from human subcutaneous WAT cells by exploring the dataset (*18*). We found that B7-H3 mRNA is predominantly expressed in preadipocytes and largely absent in adipocytes (fig. S1D). To confirm these findings, we performed flow cytometry on normal human adipose-derived stem cells (hADSCs; Lonza) isolated from lipoaspirates of one normal (nondiabetic) adult. We found that hADSCs highly expressed CD90, CD73, and B7-H3 (fig. S1E). Furthermore, we used an immunohistochemistry (IHC)–based approach to assess the expression of B7-H3 protein in adipose tissue from obese human participants. After careful assessment, we failed to observe any signal for B7-H3 positivity in human adipocytes, while B7-$H3^+$ cells were detected in areas between adipocytes, i.e., the areas that constitute the SVF (Fig. 2L). These data suggest that the immune checkpoint B7-H3 is predominantly expressed in mouse and human APs.

B7-H3 is down-regulated during AP differentiation

Having found that B7-H3 was specifically expressed in APs and absent in primary adipocytes, we tested whether B7-H3 expression was down-regulated during adipocyte development. We proposed that down-regulation of B7-H3 expression was required for differentiation of adipocytes. To test this possibility, we performed a time course analysis of gene expression during in vitro adipogenic differentiation of mouse 3T3-L1 preadipocytes, which constitutively express a high level of B7-H3 in the undifferentiated state (Fig. 2M). Provision of the adipogenic cocktail to the culture led to rapid down-regulation of mouse *B7-H3* mRNA, which remained low throughout the experiment (Fig. 2N). In contrast, peroxisome proliferator–activated receptor γ (*PPARγ*), a master regulator of adipocyte differentiation, was progressively up-regulated over time (Fig. 2N). In agreement with these findings, analysis of pooled mouse embryos during embryonic and postnatal development (*19*) showed decreased mouse *B7-H3* mRNA expression during the course of adipose tissue formation (Fig. 2O), as also observed with other APs markers such as *Sox9* (*20*). In sharp contrast, *CEBPα* (CCAAT Enhancer Binding Protein Alpha), a gene required for adipocyte commitment and differentiation, was gradually up-regulated during the course of adipocyte development (Fig. 2O). In consistency with our findings in 3T3-L1 cells, levels of human B7-H3 expression in adipose tissue–derived human stromal stem cells (*21*) were found to decrease after 7 days of adipogenic differentiation, while *PPARγ* was significantly increased (Fig. 2P). Collectively, our data indicate that, upon adipogenic differentiation, APs rapidly reduce their levels of B7-H3, suggesting that reduction of B7-H3 protein is required for adipocyte differentiation.

Lack of B7-H3 alters the transcriptional program of APs

To gain insight into the function of B7-H3 in APs, we performed RNA-seq analysis of APs isolated from either WT controls or whole-body B7-H3 knockout (KO) mice. Total RNA was purified

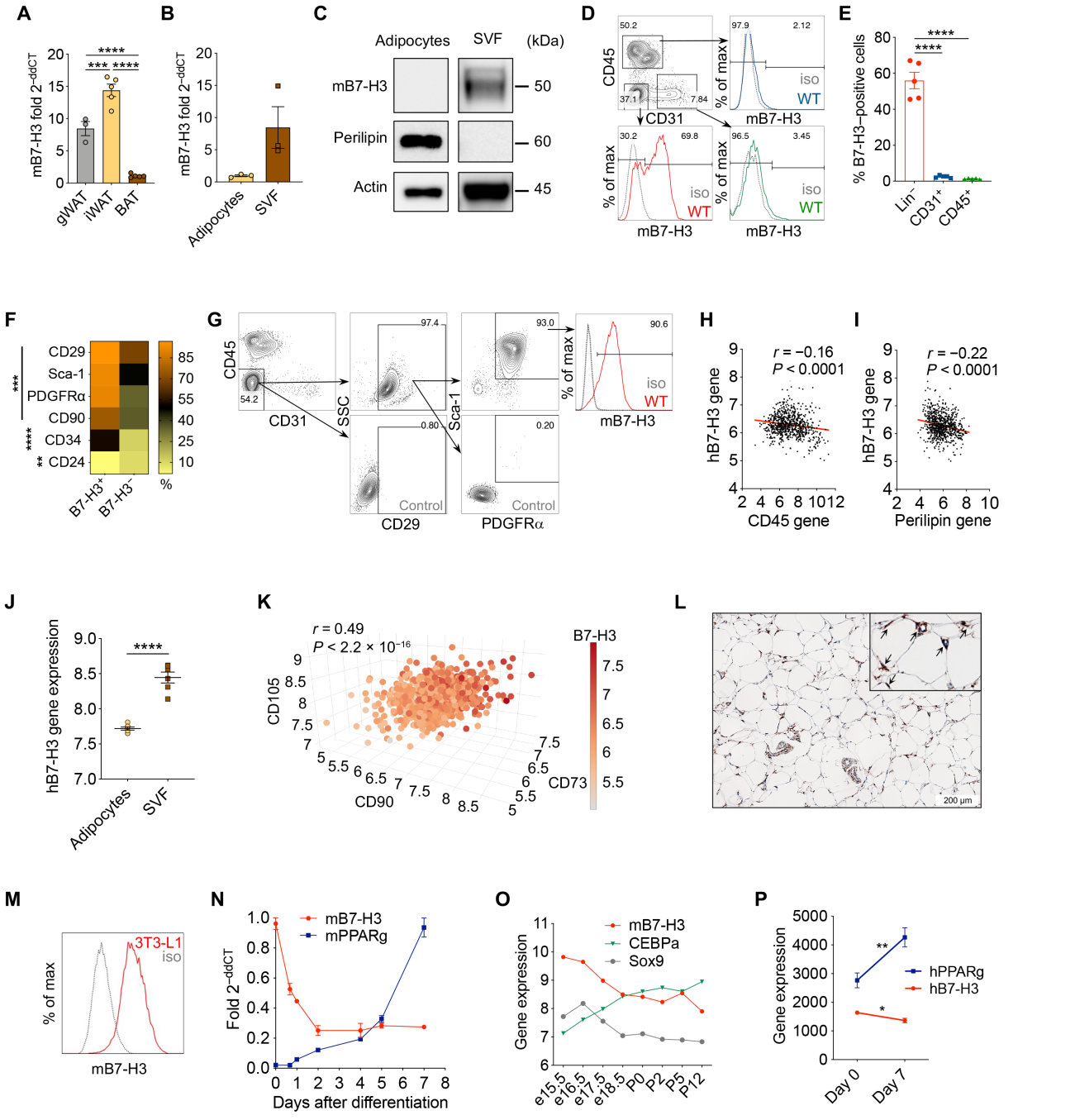

Fig. 2. B7-H3 is highly expressed in mouse and human APs. (**A**) B7-H3 mRNA in gWAT ($n = 3$), iWAT ($n = 5$), and BAT ($n = 5$) of mice. (**B**) B7-H3 mRNA in primary adipocytes and SVF from mouse gWAT ($n = 3$). (**C**) B7-H3, perilipin, and actin by Western blot on primary adipocytes and SVF from mouse gWAT ($n = 1$). (**D** and **E**) Flow cytometry of SVF from mouse gWAT ($n = 5$). Staining (D) and average expression (E) of B7-H3 in $CD45^+$, $CD31^+$, and $CD45^-CD31^-$ (Lin^-) cells. (**F**) Heatmap of classical stem/progenitor markers expression by B7-$H3^+$ and B7-$H3^-$ Lin^- cells. (**G**) B7-H3 on $CD29^+Sca\text{-}1^+PDGFR\alpha^+$ mouse APs. (**H** and **I**) B7-H3–negative correlation with CD45 (H) and adipocyte marker perilipin (I) in the METSIM study ($n = 770$) [GSE70353s (*10*)]. The red line represents nonlinear regression with straight line fitting. (**J**) B7-H3 gene expression in primary adipocytes ($n = 4$) and SVF ($n = 5$) from subcutaneous WAT of nonobese individuals [GSE80654 (*17*)]. (**K**) B7-H3–positive correlation with adipose-derived stem cell (ADSC) markers CD105, CD90, and CD73 in the METSIM study ($n = 770$). (**L**) B7-H3 IHC of subcutaneous fat from obese individuals ($n = 14$). Arrows indicate positive staining area. (**M**) Flow cytometry plot of B7-H3 on 3T3-L1 preadipocytes ($n = 5$). iso, isotype. (**N**) B7-H3 and PPARγ mRNA expression in 3T3-L1 during adipogenic differentiation ($n = 2$). (**O**) B7-H3, CEBPα, and Sox9 expression in mouse WAT from embryonic stage e15.5 to day 12 after birth [GSE29502 (*19*)]. P0, postnatal day 0. RNA from developing WAT pooled from four independent embryos ($n = 4$). (**P**) B7-H3 and PPARγ mRNA in human adipose-derived stromal stem cells before ($n = 5$) and after ($n = 4$) 7 days of adipogenic differentiation [GSE61302 (*21*)]. Data are represented as means ± SEM. For (A), (C), (E), and (F), one representative experiment of two independent experiments is shown. Data were analyzed by one-way ANOVA (A and E), Pearson correlation (H, I, and K), and Student's *t* test (B, F, J, and P). $^*P < 0.05$, $^{**}P < 0.01$, $^{***}P < 0.001$, and $^{****}P < 0.0001$.

from WT or B7-H3 KO APs freshly purified by fluorescence activated cell sorting (FACS) from three pooled gWAT for each sample. Principal components analysis demonstrated that APs from WT and KO mice clustered in distinct groups (fig. S2A). Upon differentially expressed gene (DEG) analysis, we identified a total of 152 genes with significant expression changes: 50 and 102 genes were up- and down-regulated, respectively, in B7-H3 KO compared to WT APs (table S1). Unsupervised hierarchical clustering displayed a unique set of DEGs in KO APs compared to WT AP cells (Fig. 3A). Unbiased gene set enrichment analysis (GSEA) was then performed with Hallmark, Kyoto Encyclopedia of Genes and Genomes (KEGG) pathway, and Gene Ontology–Biological Process (GO-BP) gene set collections in the Molecular Signatures Database. These revealed that, while only two pathways were significantly up-regulated in B7-H3 KO progenitors as compared to control cells (tables S2 and S3), most pathways were significantly down-regulated in the B7-H3 KO APs (table S4). The top 10 pathways down-regulated in B7-H3 KO APs for each collection are displayed in Fig. 3B. Multiple gene sets including those associated with ribosomal, proteasomal, unfolded protein response, translation initiation, and protein folding pathways were affected, suggesting cell stress and reduced protein synthesis in B7-H3 KO APs (Fig. 3B). Key pathways, such as nonobese diabetic-like receptor, tumor necrosis factor–α, mammalian target of rapamycin complex 1 (mTORC1), and interleukin-6/Janus kinase/signal transducer and activator of transcription 3 (IL-6/JAK/STAT3) signaling pathways were found to be down-regulated in B7-H3 KO APs. Among these, mTORC1 is a master regulator of cellular growth and metabolism and is associated with proglycolytic metabolism (*22*). *Myc*, another proglycolytic factor, was also a part of the DEG list (Fig. 3A and table S1) (fold change of −3.67 KO versus WT), and Myc target genes were found to be underrepresented in genes of higher expression in B7-H3 KO APs (Fig. 3B). The myc network has been shown to control multiple functions, including cell proliferation, differentiation, growth, and metabolism (*23*). Consequently, we narrowed our analysis to the physiologically significant metabolic gene sets and found that carbohydrate (glycolysis), lipid [fatty acid (FA) metabolism], and amino acid (regulation of cellular amino acid metabolic process) metabolism were largely impaired in B7-H3 KO APs with respect to WT APs (Fig. 3C), suggesting that B7-H3 protein globally controls substrate utilization in APs. The expression of FA oxidation genes was not decreased in B7-H3 KO APs (fig. S2B). However, mitochondrial oxidative phosphorylation, tricarboxylic acid cycle, and adenosine triphosphate (ATP) synthesis were each dysregulated in B7-H3–deficient APs when compared to WT progenitors (Fig. 3C). The list of genes that contributed to the enrichment of metabolic pathways in B7-H3 KO cells is provided in table S5. Together, our transcriptomic analyses indicate that B7-H3 is broadly required for stimulation of diverse molecular pathways that typically associate with protein biosynthesis and metabolic regulation, and, perhaps in this way, B7-H3 broadly maintains the identity of AP cell.

B7-H3 stimulates glycolytic and oxidative metabolism in APs

To determine whether the differences in the transcriptomic program translate into functional changes, we compared the metabolic activities of APs isolated from WT and B7-H3 KO mice in an ex vivo scenario. To that purpose, we performed a Seahorse glycolysis stress test (GST) to measure glycolytic activity in isolated cells. Extracellular acidification rate (ECAR) and oxygen consumption rate (OCR) were measured as indicators of cellular glycolysis and mitochondrial respiration, respectively. Consistent with our transcriptomic data, in response to GST, KO cells showed only a modest increase in ECAR after injection of saturating amounts of glucose when compared to WT cells (Fig. 4A). While injected oligomycin, which inhibits ATP-coupled respiration, led to further increases in ECAR in control cells, ECAR tended to be dampened in oligomycin-injected B7-H3 KO APs (Fig. 4A). Because both glycolysis and glycolytic capacity, albeit to a lower extent, of B7-H3 KO APs were largely impaired (Fig. 4B), these data suggest that B7-H3 plays a role in stimulating glycolytic function in APs.

To further confirm that B7-H3 stimulates glycolysis, we performed loss-of-function and gain-of-function study using an immortalized preadipocyte cell line, Ing-svf, which was established from SVF cells isolated from iWAT of C57BL/6 mice (*24*). We sought to use the Ing-svf cell line to ensure that changes in glycolysis are due to cell-intrinsic effect of loss of B7-H3 and not secondary to a cell nonautonomous regulation in vivo. To knock out B7-H3 in vitro, we transduced Ing-svf cultures with lentiCRISPRv2 constructs containing scramble nontargeted or B7-H3–targeted CRISPRko single guide RNAs (sgRNAs). Transduced cells were stained for B7-H3 and FACS-sorted into stable populations of control and B7-H3 KO Ing-svf cells (fig. S3A). Consistent with our findings in B7-H3 KO APs, B7-H3 KO Ing-svf cells were also less glycolytic, albeit modestly, when compared to the control cell line (Fig. 4, C and D). We confirmed these results by overexpressing B7-H3. To this end, we transduced Ing-svf cells with control or B7-H3–expressing pHIVzgreen lentivirus. Zgreen^{+} fluorescent cells were then FACS-sorted into stable population of control and B7-H3^{high} Ing-svf cells (fig. S3B). As expected, increasing B7-H3 expression in cells resulted in significantly higher glycolytic activity in Ing-svf preadipocytes compared to controls (Fig. 4, E and F). In addition, B7-H3–driven increases in glycolysis correlated with increased oxidative metabolism in APs. When compared to controls cells, basal OCR was lower both in B7-H3 KO APs (Fig. 4G) and in KO Ing-svf cells (Fig. 4H). These differences were maintained despite glucose administration (Fig. 4, G and H), suggesting that B7-H3 controls glucose-mediated OCR by APs. B7-H3 has been shown to regulate glycolysis in cancer cells through modulation of cellular ROS levels and HIF1α stability (*3*). Here, we noted that ROS levels tended to decrease in B7-H3 KO APs compared to WT APs (fig. S3C). Furthermore, B7-H3 KO APs had significantly lower mitochondrial mass [as measured by MitoTracker Green staining (*25*)] (fig. S3D) and mitochondrial membrane potential [as measured by MitoTracker Deep Red staining (*25*)] (fig. S3E) compared to WT APs. Together, our data confirm that cell-intrinsic B7-H3 drives glycolysis and oxidative metabolism in APs.

Lack of B7-H3 in APs alters oxidative program and lipid storage in derived adipocytes

It has been described that the metabolic program in stem and progenitor cells differs from the one observed in differentiated cells (*26*, *27*). While APs exhibit high glycolytic activity, differentiated adipocytes exhibit a program based on oxidative metabolism (*28*). Oxidative metabolism is a key for adipocytes' biology because it is tightly associated with both β-oxidation and storage of fat (*29*). Consistent with this idea, we observed a marked decrease in glycolysis as WT APs (high glycolytic rates) differentiated into corresponding adipocytes (low glycolytic rates), while the change was minimal for B7-H3 KO cells (Fig. 5A).

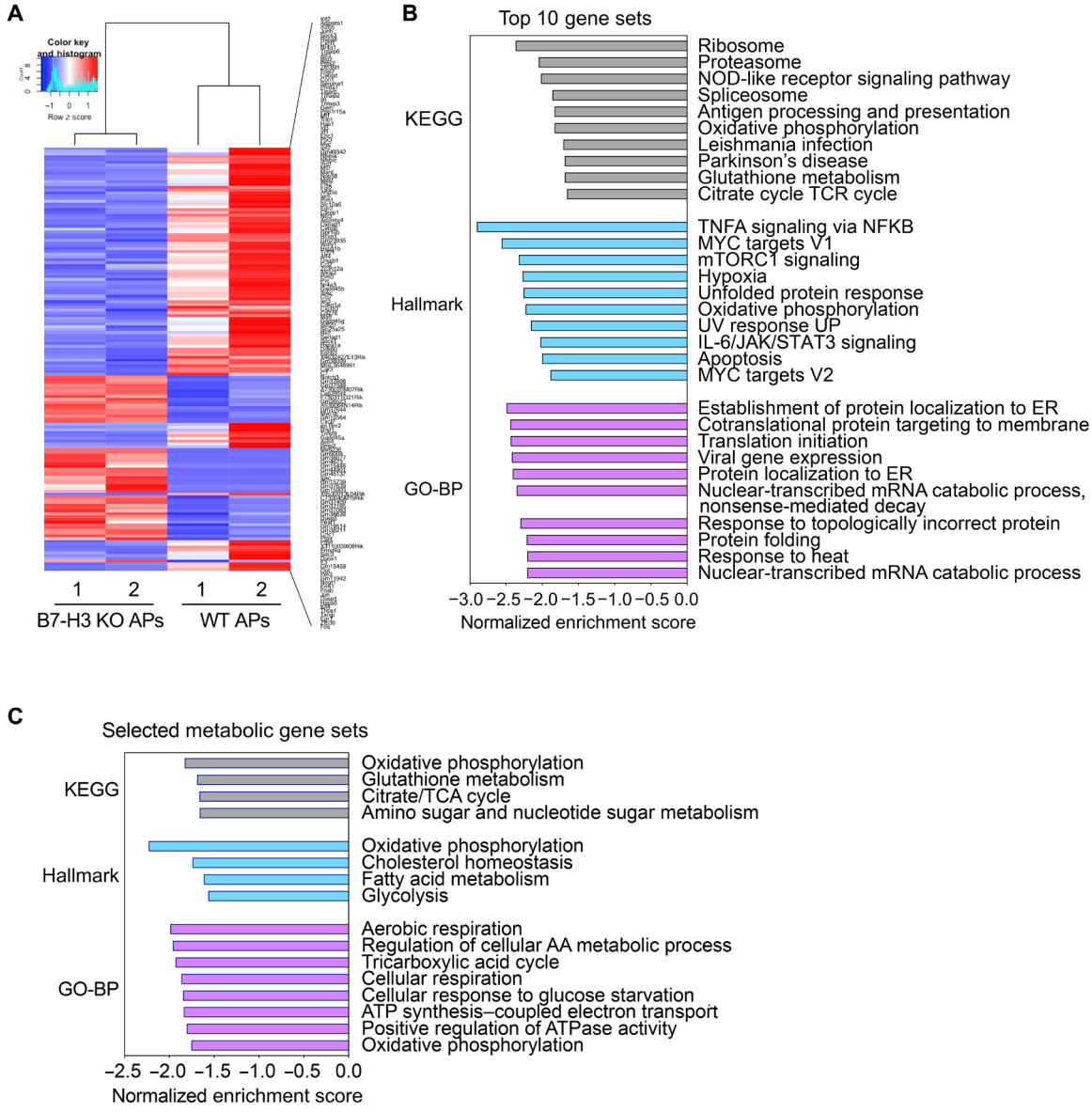

Fig. 3. Lack of B7-H3 alters the transcriptional program of APs. (**A** to **C**) RNA-seq was performed on APs purified by FACS from gWAT of age- and weight-matched WT ($n = 2$) and B7-H3 KO ($n = 2$) mice. For each sample, gWAT was pooled from three mice before enzymatic digestion, staining, sorting, and RNA purification. (A) Heatmap of DEGs (>2-fold) between WT and B7-H3 KO APs. (B and C) Pathway and gene sets enriched in genes down-regulated in B7-H3 KO compared to WT APs. GSEA was performed to identify KEGG, Hallmark, and GO-BP sets that were significantly enriched (false discovery rate < 0.05) for genes down-regulated in B7-H3 KO APs. Top 10 pathways (B) and selected metabolic gene sets (C) are listed and ranked on the basis of normalized enrichment score.

To test whether metabolic gene alterations in progenitors were maintained in derived adipocytes, we analyzed the expression of 84 key genes involved in mitochondrial respiration, including genes encoding components of the electron transport chain and oxidative phosphorylation complexes, in WT and B7-H3 KO differentiated adipocytes by using the RT^2 Profiler Mitochondrial Energy Metabolism qPCR Array (QIAGEN). Most of the significantly down-regulated genes in B7-H3 KO adipocytes were subunits (*Nduf* genes) of the mitochondrial complex I {NADH [reduced form of nicotinamide adenine dinucleotide (NAD)]–coenzyme Q reductase} (Fig. 5B and table S6). *Cox11*, *Atp4a*, and *Atp4b* are part of the mitochondrial complex IV (ATP synthase), while *Uqcrh* is part of the mitochondrial complex III (coenzyme Q–cytochrome c reductase) (Fig. 5B). Thus, we confirmed that metabolic gene alterations found in B7-H3–deficient progenitors (Fig. 3C and table S5) were conserved in differentiated adipocytes. Consistently, while their glycolytic capacity was not altered (Fig. 5C), we observed that the OCR was reduced in adipocytes derived from B7-H3 KO APs (Fig. 5D), suggesting that loss of B7-H3 in APs affects the oxidative program in derived adipocytes.

To test whether B7-H3–driven metabolic programming of APs and adipocytes regulates fat storage, we compared lipid accumulation in WT and B7-H3 KO adipocytes after 10 days of differentiation by staining neutral lipid droplets with both HCS LipidTOX Red reagent

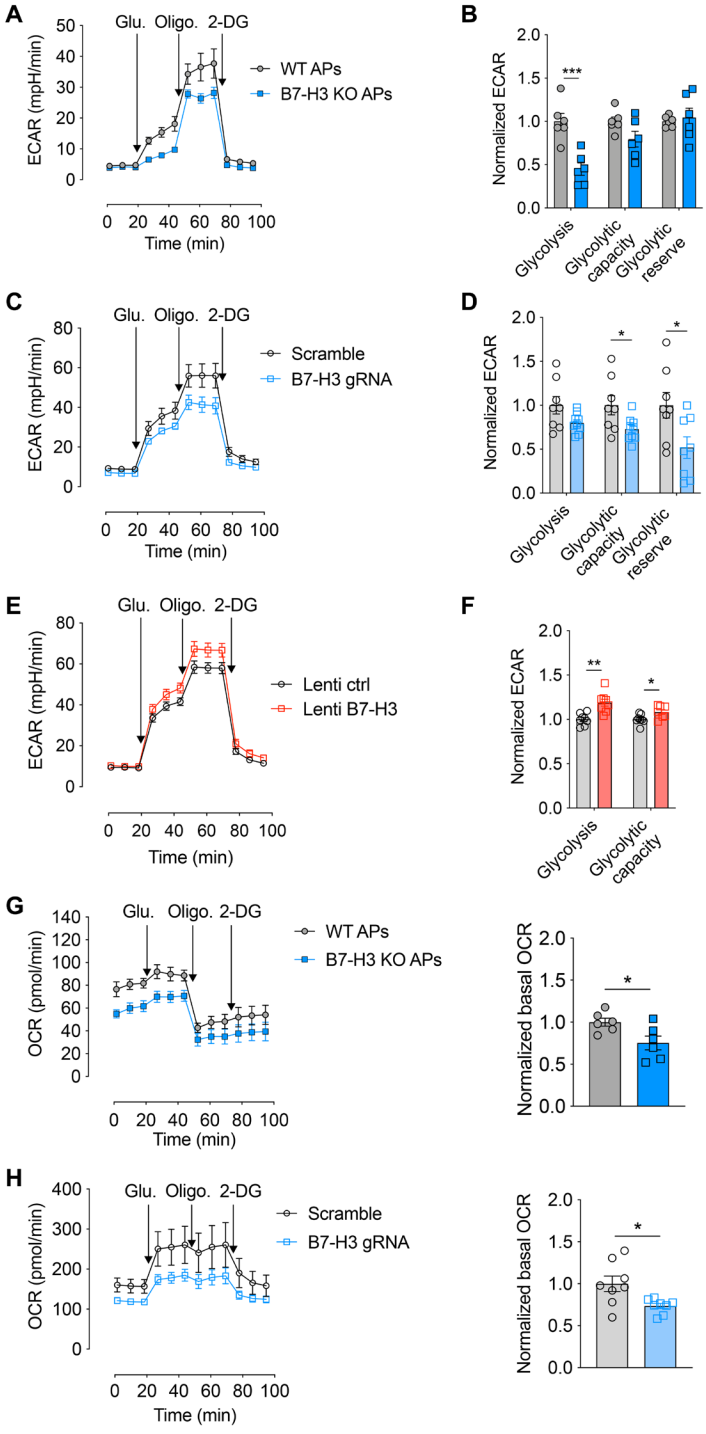

Fig. 4. B7-H3 promotes AP glycolytic and oxidative metabolism. (**A** and **B**) GST on APs isolated from iWAT of WT ($n = 6$) and B7-H3 KO mice ($n = 6$). Cells were isolated by positive magnetic selection and passaged once. (A) Glucose (Glu.), oligomycin (oligo.), and 2-deoxyglucose (2-DG) were sequentially injected while the ECAR was measured over time. (B) Glycolysis, glycolytic capacity, and glycolytic reserve were calculated. (**C** and **D**) Ing-svf cell line, derived from immortalized SVF from WT mouse iWAT, (Ing-svf) was transduced with two nontargeted scrambles or two B7-H3–targeted sgRNA lentiCRISPRv2 viruses to generate two stable control and two B7-H3 KO Ing-svf cell lines. GST was performed on transduced FACS-sorted cell lines ($n = 2$). (C) Glucose (Glu.), oligomycin (oligo.), and 2-DG were sequentially injected, while the ECAR was measured over time. (D) Glycolysis, glycolytic capacity, and glycolytic reserve were calculated. (**E**) Ing-svf was transduced with control or B7-H3–encoding pHIVzgreen lentivirus to generate stable control and B7-H3^{high} Ing-svf cell lines. GST was performed on transduced FACS-sorted cell lines ($n = 2$). (**F**) Glycolysis and glycolytic capacity were calculated. (**G**) OCR of APs isolated from iWAT of WT ($n = 6$) and B7-H3 KO ($n = 6$) mice during GST (left). Basal OCR is shown on the right. (**H**) OCR of scramble and B7-H3 gRNA lenti-transduced Ing-svf during GST ($n = 2$) (left). Basal OCR is shown on the right. Data are represented as means ± SEM between two independent experiments and are normalized to the mean of the control values for each experiment [for (B), (D), and (F) to (H)]. Data were analyzed by Student's *t* test with Welch correction (B, D, and F to H). *$P < 0.05$, **$P < 0.01$, and ***$P < 0.01$.

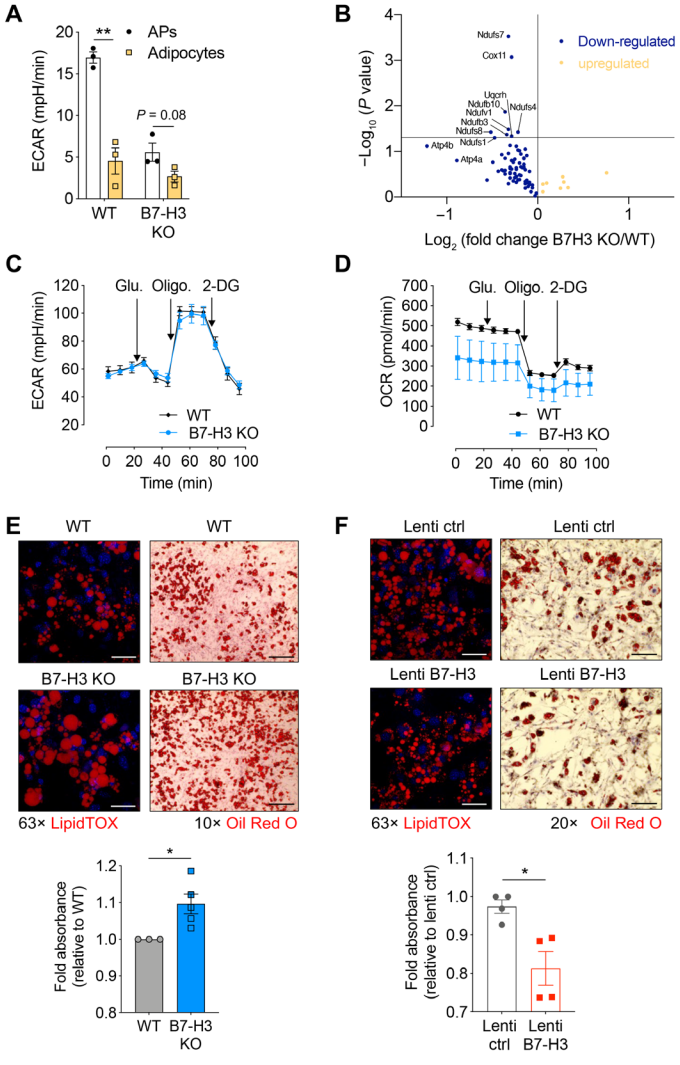

Fig. 5. Lack of B7-H3 in APs alters oxidative program and lipid storage in derived adipocytes. (**A**) GST was performed on WT ($n = 3$) and B7-H3 KO ($n = 3$) APs and derived adipocytes 7 days after induction of differentiation. Glycolysis was compared between APs and adipocytes. (**B**) Volcano plot of DEGs between WT ($n = 4$) and B7-H3 KO ($n = 4$) adipocytes 9 days after induction of differentiation. (**C** and **D**) GST on WT ($n = 3$) and B7-H3 KO ($n = 3$) adipocytes 7 days after induction of differentiation. Glucose (Glu.), oligomycin (oligo.), and 2-DG were sequentially injected, while ECAR (C) and OCR (D) were measured over time. (**E**) HCS LipidTOX Red (top left) and ORO (top right) representative staining of iWAT WT ($n = 3$) and B7-H3 KO ($n = 5$) APs after 9 days of differentiation to adipocyte lineage and quantification of ORO absorbance (bottom). Scale bars, 50 μm (white) and 200 μm (black). (**F**) HCS LipidTOX Red (top left) and ORO (top right) representative staining of control ($n = 2$) and B7-H3–overexpressing ($n = 2$) Ing-svf after 9 days of differentiation to adipocyte lineage and quantification of ORO absorbance (bottom). Scale bars, 50 μm (white) and 200 μm (black). Data are represented as means ± SEM from one (A, C, and D), two (B and E), and three (F) independent experiments. Data were analyzed by one-sample *t* test (E) and Student's *t* test (A, B, and F). $^*P < 0.05$ and $^{**}P < 0.01$.

and Oil Red O (ORO) dye. We observed that B7-H3 KO adipocytes displayed a small but significantly increased accumulation of neutral lipids per cell compared to WT cells (Fig. 5E). To determine whether these differences were due to increased KO adipocyte differentiation, we quantified the gene expression levels of progenitor- and adipocyte-specific markers, as well as adipogenic factors, in both nondifferentiated APs and adipocytes at day 9 of adipogenesis. We found that progenitor markers *PDGFRα* and *Sca1* were expressed at a similar level in WT and B7-H3 KO progenitors and were down-regulated with differentiation to adipocytes (fig. S4A). Master regulators of adipogenesis *Pparγ* and *Cebpα*, as well as FA and glucose transporters *Fabp4* and *Glut4*, were similarly up-regulated in WT and B7-H3 KO adipocytes (fig. S4B), indicating no difference in adipogenesis between the two groups. Furthermore, isolated WT and B7-H3 KO APs showed comparable proliferation, as measured by cell counting kit (CCK) assay ex vivo (fig. S4C).

We confirmed these results by overexpressing B7-H3. While their differentiation was similar (fig. S4D), B7-H3–overexpressing Ing-svf cells displayed reduced lipid accumulation as compared to control Ing-svf cells (Fig. 5F). Together, these results suggest that the expression of B7-H3 in APs serves to imprint an oxidative program in their differentiated progeny, thereby limiting fat storage.

B7-H3 KO mice develop spontaneous obesity

Because B7-H3 alters metabolism and fat storage, we hypothesized that the absence of B7-H3 would lead to accrual of fat and onset of obesity. To test this possibility, we measured body weight over time in age-matched B7-H3 KO and WT control mice that were fed a regular chow diet that contains 9% crude fat (PicoLab, 5058). We observed that both B7-H3 KO male and female mice gained significantly more weight, being 60% heavier than WT controls at 4 months of age (Fig. 6, A and B). Body weights diverged early on, around 7 weeks of age for females and 10 weeks for males. To rule out potential differences in the genetic background, we backcrossed B7-H3 KO mice to WT mice and confirmed that rederived B7-H3 KO mice gained significantly more weight than B7-H3$^{+/+}$ littermate controls (fig. S5A). To determine whether obesity also develops with a lower fat chow diet, we fed mice with a 4.5% crude fat diet (PicoLab, 5053) and observed that body weights of B7-H3 KO mice increased after 15 weeks compared to control mice for both genders (fig. S5B). Furthermore, feeding mice with a HFD with 60% calories provided by fat (TestDiet, 58Y1) exacerbated weight gain in B7-H3 KO mice when compared to controls (Fig. 6C). Mice knocked out for another immune checkpoint of the B7 family—PD-L1 (Programmed death-ligand 1), recently reported as a marker of brown fat (*30*)—showed no body weight difference as compared to WT mice under HFD (fig. S5C), confirming a unique role for B7-H3 in controlling body weight gain.

To assess whether lack of B7-H3 induces excessive fat accumulation in vivo, we performed quantitative nuclear magnetic resonance (NMR) (Fig. 6D) and computed tomography (CT) scanner imaging (Fig. 6E). Compared to controls, B7-H3 KO mice displayed increased fat mass, notably in the visceral and subcutaneous regions, while no change in lean mass was observed. Given the development of adiposity in B7-H3 KO mice, we sought to compare the weight and size of different mouse fat depots to determine whether fat accrual occurred in specific depot. We found that gWAT, iWAT, and BAT depots from 4-month-old B7-H3 KO mice were heavier and larger than those from WT mice (Fig. 6F). Histological analysis of WAT was performed to study adipocyte hypertrophy. We observed that adipocytes from B7-H3 KO gWAT were significantly larger in size than WT cells with an average area twice the size of WT cells (Fig. 6G). WT adipocytes were largely characterized by smaller cell area (<4000 μm^2), while the B7-H3 KO cells displayed

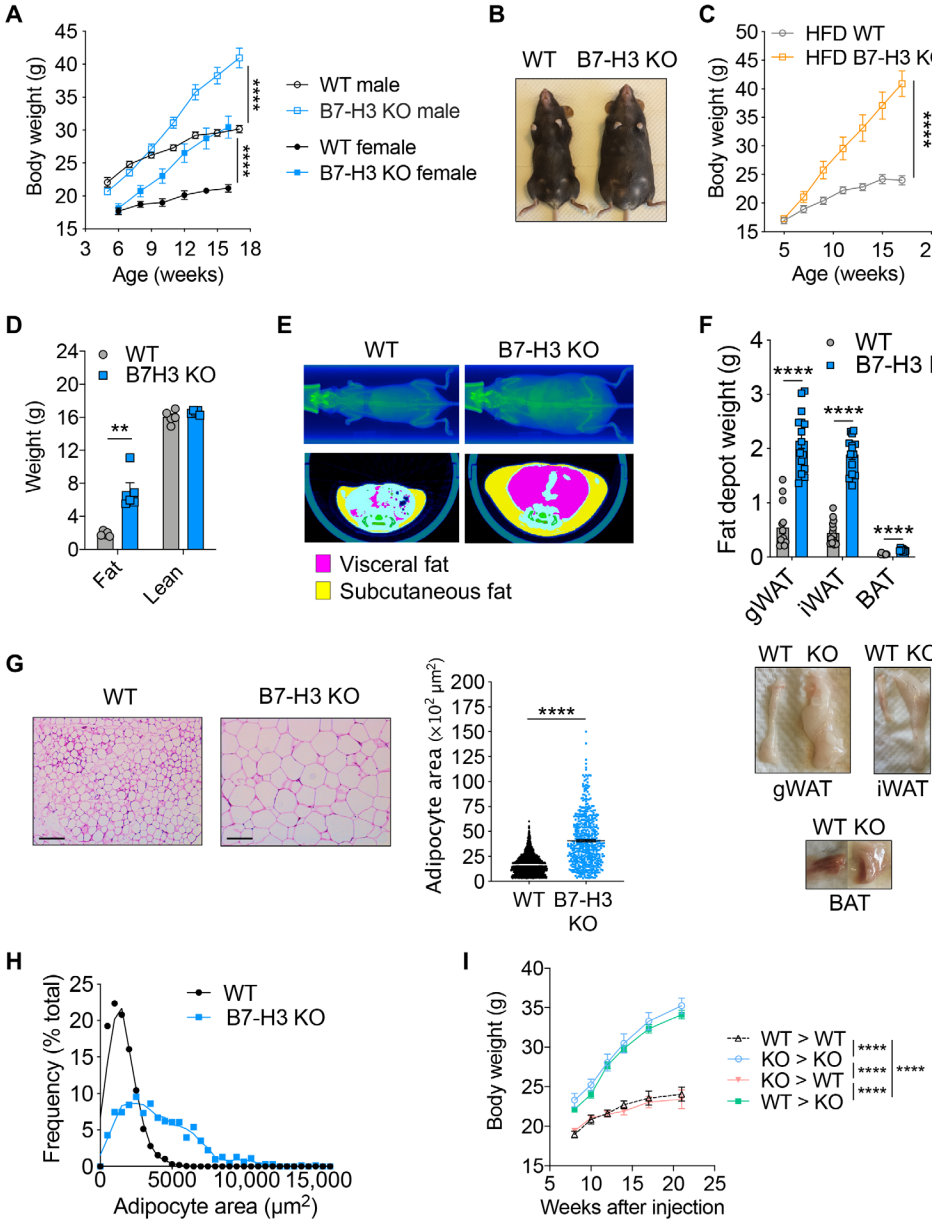

Fig. 6. B7-H3 KO mice develop spontaneous obesity. (**A**) Body weight of WT male ($n = 10$), B7-H3 KO male ($n = 10$), WT female ($n = 10$), and B7-H3 KO female ($n = 10$) mice fed a normal chow (9% crude fat). (**B**) Picture of WT and B7-H3 KO female mice fed a normal chow (9% crude fat). (**C**) Body weight of WT ($n = 10$) and B7-H3 KO ($n = 10$) female mice fed with HFD (60% fat). (**D**) Body composition of 4-month-old WT ($n = 5$) and B7-H3 KO ($n = 5$) female mice measured by magnetic resonance imaging. (**E**) Fat distribution of 4-month-old WT ($n = 5$) and B7-H3 KO ($n = 5$) female mice measured by CT scan. One representative mouse is shown. (**F**) Weight and size of WT and B7-H3 KO gWAT (WT, $n = 14$; KO, $n = 15$), iWAT ($n = 14$ each group), and BAT ($n = 8$ each group) from 4-month-old mice. (**G**) Hematoxylin and eosin (H&E) staining of gWAT histological sections from 4-month-old WT ($n = 5$) and B7-H3 KO ($n = 5$) mice. One representative image is shown on the left. A minimum of 100 adipocytes per mouse were quantified for area (right). Scale bars, 100 µm. (**H**) Frequency distribution of adipocyte areas in gWAT. (**I**) WT and B7-H3 KO mice were irradiated before intravenous injection of either WT or B7-H3 KO BM to generate four groups of chimeric mice: WT BM > WT ($n = 5$), KO BM > KO ($n = 6$), KO BM > WT ($n = 6$), and WT BM > KO ($n = 8$). Body weight was measured over time starting 8 weeks after irradiation and BM injection. Data are represented as means ± SEM between one (D and I), two (A, C, and G), and three (F) independent experiments. Data were analyzed by two-way ANOVA (I) and Student's *t* test (A, C, D, F, and G). $^{**}P < 0.01$ and $^{****}P < 0.0001$.

broad increases in cell area as depicted in Fig. 6H. Consistent with the obesity phenotype, as expected, B7-H3 KO brown adipocytes showed higher lipid content and bigger lipid droplets than WT cells, indicating the "whitening" of brown fat (fig. S5D). Obesity development in B7-H3 KO mice remained independent of changes in feeding, because both young and older age-matched WT and B7-H3 KO mice had similar daily food intake (fig. S5, E and F), with comparable meal number, meal size, meal interval, and satiety ratio and shorter meal duration in B7-H3 KO mice (fig. S5G). To test whether lack of B7-H3 increases absorption of dietary lipids, we subjected WT and B7-H3 KO mice to an oil gavage after overnight fasting. The amounts of serum triglyceride (TG) detected at 1, 2,

and 6 hours after gavage were similar between the two groups, suggesting similar lipid absorption (fig. S5H). Furthermore, energy expenditure measured by indirect calorimetry at 5 weeks of age (fig. S5I) and 16 weeks of age (fig. S5J) was comparable between WT and B7-H3 KO mice. Consistent with our findings ex vivo in fig. S4B, we detected similar gene expression of *PPARγ*, FA-binding protein 4 (*FABP4*), and *CEBPα* in gWAT from WT and B7-H3 KO mice (fig. S5K), suggesting no difference in adipogenesis in vivo. Last, while physical activity was found to be similar in both groups at 5 weeks of age (fig. S5L), activity showed a tendency to decrease in the B7-H3 KO animals at 16 weeks of age (fig. S5M), likely, in part, because of their higher body weights. Hence, changes in energy intake, systemic energy expenditure, adipogenesis, and physical activity are likely not the primary determinant of adiposity in B7-H3 KO mice.

As microbiota is involved in obesity development in some mouse models (*31*–*33*), we evaluated its potential role in the increased adiposity observed in B7-H3–deficient animals. We found that modulating microbiota either by broad-spectrum antibiotics treatment or cohousing mice (fig. S6A) did not prevent the onset of obesity nor transfer it to control animals, suggesting that the gut microbiota is not a major contributor to the obesity observed in B7-H3 KO mice. Together, our results demonstrate that lack of B7-H3 in mice induces substantial fat storage and spontaneous obesity despite feeding a nonobesogenic regular chow diet and independently of the gut microbiome.

Nonimmune parenchymal cell-intrinsic B7-H3 expression protects against obesity

We showed earlier that the highest expression of B7-H3 is found in WAT, specifically in APs. Mouse B7-H3 protein is absent in other organs regulating metabolism such as liver, skeletal muscle, and brain (*34*). However, it is expressed by certain immune cells, such as activated dendritic cells and macrophages (*1*), which contribute to regulate metabolism. To test whether B7-H3–protective effect on obesity was intrinsic to APs and/or immune cells, we generated bone marrow (BM) chimeric mice. BM cells from WT or B7-H3 KO donor mouse were injected into either WT or B7-H3 KO irradiated young recipient mice. First, we confirmed that B7-H3 KO mice reconstituted with KO BM developed obesity compared to WT controls receiving WT BM (Fig. 6I). However, reconstitution of irradiated B7-H3 KO mice with WT BM (i.e., B7-H3 expressed on immune cells but absent on tissue cells) failed to prevent excessive body weight gain (Fig. 6I). Furthermore, WT mice that received KO BM (i.e., B7-H3 expressed on tissue cells but absent on immune cells) remained lean over time. Together, these data confirm that B7-H3 expression on radio-resistant tissue cells, but not on cells from hematopoietic origin, protects against obesity.

Innate and adaptive immunity do not contribute to obesity onset in B7-H3 KO mice

Because B7-H3 plays an important function in regulating immunity (*35*), we sought to determine the contribution of the innate immune signaling to the excessive weight gain in B7-H3 KO mice. To do this, we generated BM chimeras using MyD88$^{-/-}$ donor mice. B7-H3 KO mice reconstituted with either WT or MyD88$^{-/-}$ BM developed obesity at a similar rate when compared to WT lean recipients injected with WT or MyD88$^{-/-}$ BM (fig. S6B). Thus, impairment of the BM-derived TLR-MyD88 signaling in the B7-H3 KO mice does not appear to protect from obesity. Furthermore, because one major function of B7-H3 is to inhibit T cell activity in mouse and human (*36*, *37*), we tested the contribution of T cells and natural killer T (NKT) cells to the development of obesity in our B7-H3 KO mice. To this purpose, we crossed the B7-H3 KO mice to Rag1 KO immunodeficient mice, which lack T cells, B cells, and NKT cells, to generate double KO mice and compared body weight gain and adiposity over time. We found that both male and female Rag1.B7H3 KO mice developed obesity (fig. S6, C and D) with larger liver, iWAT, and gWAT (fig. S6E) compared to Rag1 KO control mice. Together, these results show that modulating the innate or adaptive immune system does not prevent obesity development, suggesting that nonimmune function of B7-H3 is the key to control adiposity.

Loss of B7-H3 reduces lipolysis and fat oxidation in adipose tissue before obesity onset

Adipocyte lipid content is regulated positively by FA uptake, esterification, and de novo lipogenesis and regulated negatively by lipolysis and FA oxidation. Notably, B7-H3 was shown to regulate lipid metabolism of lung cancer cells (*38*). To determine whether the mechanism by which loss of B7-H3 causes adiposity is, in part, via modifying lipid metabolism in adipocytes, we studied these distinct pathways by analysis of gene expression in gWAT and in vivo and ex vivo functional assays in young animals. At 5 weeks of age, before the onset of obesity, we observed no difference in the expression levels of key lipogenic genes FA synthase (*FAS*), stearoyl–coenzyme A (*CoA*) desaturase-1 (*SCD1*), ATP citrate lyase (*ACLY*), and carbohydrate-responsive element-binding protein (*ChREBP*) (fig. S7A). Sterol regulatory element binding protein 1 (*SREBP1*) was significantly downregulated in the B7-H3 KO fat pad (fig. S7A). We found no difference in expression of the lipolytic enzyme lipoprotein lipase (*LPL*) (Fig. 7A) between WT and B7-H3 KO groups. However, when mice were injected with a β-adrenergic agonist to induce lipolysis (isoproterenol), we noted a decrease in glycerol release in B7-H3 KO mice (Fig. 7B). This suggests that B7-H3 KO adipocytes exhibit lower response to lipolytic stimuli than WT cells. The enzyme *PEPCK* (Phosphoenolpyruvate carboxykinase) involved in FA reesterification was expressed at similar levels in both WT and B7-H3 KO tissues (fig. S7B). Unexpectedly, gene expression of *FABP* and FA transporter *CD36* in gWAT was significantly decreased in the B7-H3 KO compared to WT mice (fig. S7C). Collectively, these results suggest a partial role for B7-H3 in regulating lipolysis in adipocytes before obesity onset.

As we observed metabolic deregulations in both B7-H3 KO APs and derived adipocytes ex vivo (Figs. 4 and 5), we evaluated whether these dysfunctions were conserved in mice. The gene expression of *HK2*, an enzyme involved in the first step of glycolysis, was significantly decreased in gWAT of B7-H3 KO mice, confirming the defective glycolysis at the tissue level (Fig. 7C). We then studied whether mitochondrial activity was decreased in B7-H3 KO adipose tissue as compared to WT controls by conducting respirometry analysis on tissue explants ex vivo. Basal OCR was measured after tissue permeabilization with digitonin. gWAT from B7-H3 KO mice showed a trend toward decreased OCR as compared to WT depot (Fig. 7D). On the contrary, liver and BAT OCRs were similar (fig. S7, D and E), indicating that B7-H3 stimulates mitochondrial respiration specifically in WAT.

To test whether the reduced oxidative metabolism in B7-H3 KO WAT was associated with a decrease in the occurrence of brown-like "beige" adipocytes within WAT, a phenomenon called "beiging," we measured the expression of classical thermogenic genes in

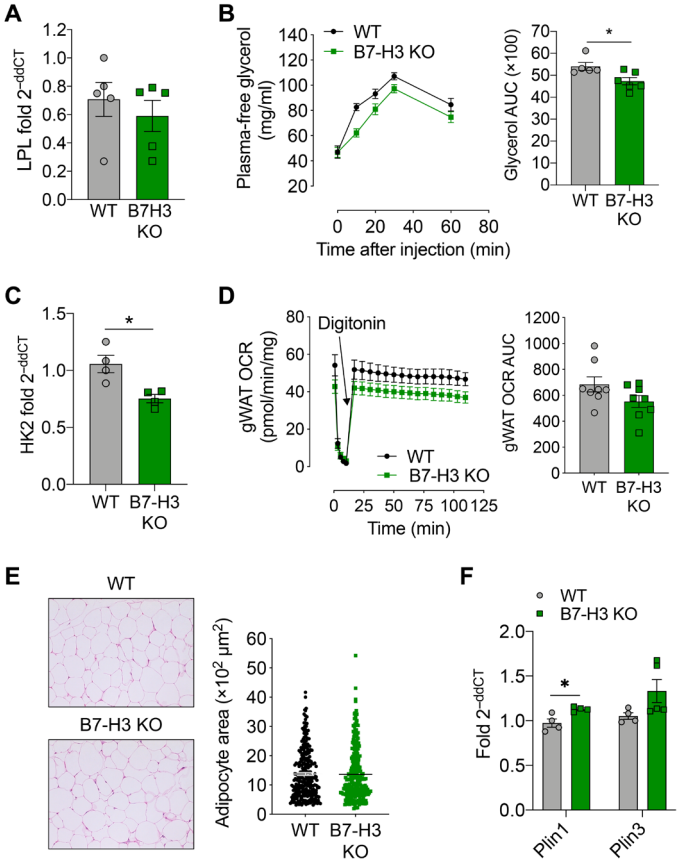

Fig. 7. B7-H3 KO adipose tissue exhibits decreased lipolysis and FA oxidation before obesity onset. (**A**) mRNA levels of lipolytic LPL in gWAT from lean 5-week-old WT ($n = 5$) and B7-H3 KO mice ($n = 5$). (**B**) In vivo lipolysis activity of 5-week-old WT ($n = 6$) and B7-H3 KO ($n = 6$) mice (left) and area under the curve (AUC) (right). Blood was collected before and after intraperitoneal injection of isoproterenol to measure plasma free glycerol over time. (**C**) mRNA level the glycolytic enzyme HK2 in gWAT from lean 5-week-old WT ($n = 5$) and B7-H3 KO mice ($n = 5$). (**D**) OCR of gWAT freshly isolated from lean 6-week-old WT ($n = 4$) and B7-H3 KO mice ($n = 4$) (left) and area under the curve (right). Digitonin was injected to permeabilize the tissue, and OCR was recorded over time. (**E**) H&E staining of gWAT histological sections from 6-week-old WT ($n = 5$) and B7-H3 KO ($n = 5$) mice. One representative image is shown on the left. A minimum of 100 adipocytes per mouse were quantified for area (bottom). Frequency distribution of adipocyte areas is shown on the right. (**F**) mRNA levels of perilipin genes in gWAT of 5-week-old WT ($n = 5$) and B7-H3 KO ($n = 5$) mice. Data are represented as means ± SEM between one (A, C, D, and F) and two (B and E) independent experiments. Data were analyzed by Student's *t* test. *$P < 0.05$.

WAT and BAT. The recently described beige adipocyte marker, proton assistant amino acid transporter-2 (*PAT2*) (*39*), showed similar expression in all tissues of both genotypes (fig. S8A). However, the transmembrane protein 26 (*Tmem26*) tended to be decreased in iWAT from B7-H3 KO mice (fig. S8B). The brown fat markers PR domain containing 16 (*Prdm16*), uncoupling protein 1 (*Ucp1*), and purinergic receptor P2X 5 (*P2RX5*) were mostly expressed in BAT with little to no expression in WAT (fig. S8, C to E). Only *P2RX5* was differentially expressed between WT and B7-H3 KO tissues, as it was down-regulated in both KO gWAT and iWAT and up-regulated in KO BAT (fig. S8E). P2RX5 is an ATP-gated ion channel, suggesting that its variable expression in the three fat tissues might correspond to energetic dysfunction.

Last, we investigated whether decreased lipolysis and oxidative metabolism associated with early signs of increased fat storage. We observed no significant difference in adipocyte size (Fig. 7E) and area distribution (fig. S8F) between gWAT from lean 5-week-old B7-H3 KO and WT mice, indicating that adipocyte hypertrophy does not precede changes in weight gain. However, discrete changes in lipid storage were already apparent at the gene expression level. Perilipin 1 (*Plin1*) and *Plin3*, regulators of lipolysis and lipid storage, were overexpressed in B7-H3 KO gWAT compared to WT gWAT (Fig. 7F). Overall, our data suggest that lack of B7-H3 is associated with decreased lipolysis and fat oxidation in WAT.

B7-H3 deficiency leads to obesity-associated systemic metabolic deregulation

Obesity is commonly associated with metabolic impairments, particularly systemic alteration of glucose metabolism. To assess the metabolic state of B7-H3 KO obese mice, we first measured levels of several indicators in the sera following overnight fasting. Fasting glucose (Fig. 8A) and insulin levels (Fig. 8B) were increased in B7-H3 KO mice compared to WT mice. Similarly, B7-H3 KO sera were enriched in TG (Fig. 8C), nonesterified free FAs (Fig. 8D), and total cholesterol (Fig. 8E). Leptin and adiponectin are two main adipokines secreted by adipocytes participating in metabolic homeostasis (*40*). We found that leptin levels were increased in serum (Fig. 8F) as well as gWAT, iWAT, and BAT from B7-H3 KO mice compared to WT mice (fig. S9A), while adiponectin levels were unchanged in gWAT and iWAT but decreased in BAT (fig. S9B). Serum leptin tended to decrease in B7-H3 KO mice at 5 weeks of age before the development of obesity (fig. S9C), but it did not significantly affect food intake as shown in fig. S5E. Thus, the hyperleptinemia seen at later stages (Fig. 8F) likely represents a compensatory secretion in response to obesity-associated leptin resistance (*41*). Next, to determine whether obesity in B7-H3 KO mice associates with defects in glucose metabolism, we performed insulin tolerance test (ITT) and glucose tolerance test (GTT) in vivo. In the ITT, insulin failed to lower the blood glucose levels in B7-H3 KO mice when compared to controls (Fig. 8G), suggesting the development of insulin resistance. Intraperitoneal GTT (IPGTT) (fig. S9D) and oral GTT (OGTT) (fig. S9E) results were similar between WT and B7-H3 KO groups, indicating preserved glucose sensitivity. However, plasma insulin levels were higher in B7-H3 KO mice during OGTT (Fig. 8H), likely as a way to compensate for the obesity-associated insulin resistance. Together, these data demonstrate that B7-H3 KO obese mice exhibit reduced sensitivity to insulin compared to control lean mice.

Similar to our study in young mice before obesity onset, we assessed the expression of glycolytic and lipid metabolism genes in gWAT from 4-month-old mice. *GAPDH* (glyceraldehyde-3-phosphate dehydrogenase), an enzyme involved in the sixth step of glycolysis, was significantly decreased in gWAT and iWAT of B7-H3 KO mice but not in BAT (Fig. 8I), confirming the defective glycolysis observed in APs ex vivo (Fig. 4) and in younger lean mice (Fig. 7C). While *FATP* mRNA remained decreased, *CD36* mRNA was slightly increased in the B7-H3 KO compared to WT tissues (Fig. 8J). We further isolated APs and differentiated them to white adipocytes that were incubated with fluorescent BODIPY FA to measure uptake over time. We observed that, upon insulin stimulation, B7-H3 KO AP-derived adipocytes displayed increased FA uptake over time as compared to WT cells (Fig. 8K), likely contributing

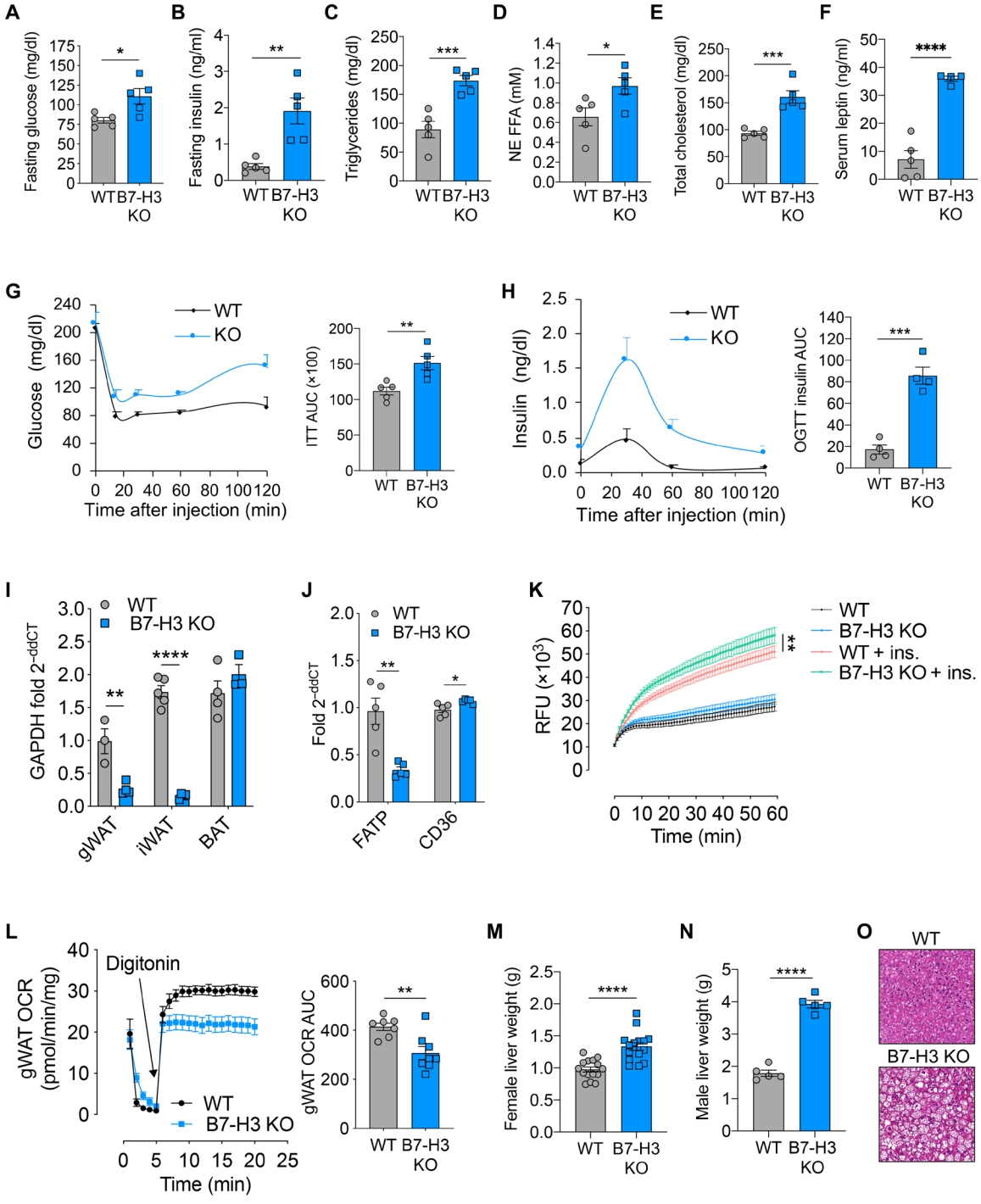

Fig. 8. B7-H3 deficiency induces systemic metabolic deregulation. (**A** to **F**) Blood biochemistry analysis after overnight fasting. (A) Serum glucose, (B) insulin, (C) TGs, (D) nonesterified free FAs (NE FFA), (E) total cholesterol, and (F) leptin were compared between 5-month-old WT ($n = 5$) and B7-H3 KO mice ($n = 5$). (**G**) ITT after 5 hours of fasting on 4-month-old WT ($n = 5$) and B7-H3 KO ($n = 5$) mice and area under the curve. Blood glucose was measured before and after intraperitoneal injection of lean mass of insulin (0.5 U/kg). (**H**) OGTT after 12 hours of fasting on 4-month-old WT ($n = 5$) and B7-H3 KO ($n = 5$) mice and area under the curve. Plasma insulin was measured before and after oral gavage of lean mass of glucose (1 g/kg). (**I**) GAPDH mRNA expression in gWAT ($n = 3$ to 4), iWAT ($n = 4$ to 5), and BAT ($n = 3$ to 4) from WT and B7-H3 KO mice. (**J**) mRNA levels of FA transport genes in gWAT from 10-month-old WT ($n = 5$) and B7-H3 KO ($n = 5$) mice. (**K**) FA uptake of adipocytes differentiated from APs of WT ($n = 6$) and B7-H3 KO ($n = 6$) mice ex vivo with or without insulin (ins.) stimulation for 1 hour before the assay. RFU, relative fluorescence units. (**L**) OCR of gWAT freshly isolated from 4-month-old WT ($n = 4$) and B7-H3 KO mice ($n = 4$) and area under the curve. Digitonin was injected to permeabilize the tissue, and OCR was recorded over time. (**M**) Liver weight of 5-month-old WT ($n = 15$) and B7-H3 KO ($n = 15$) female mice. (**N**) Liver weight of 7-month-old WT ($n = 5$) and B7-H3 KO ($n = 5$) male mice. (**O**) Representative H&E staining of male liver histological sections. Data are represented as means ± SEM between one (A to J and N), two (K and L), and three (M) independent experiments. Data were analyzed by two-way ANOVA (K) and Student's *t* test (A to J and L to N). *$P < 0.05$, **$P < 0.01$, ***$P < 0.001$, and ****$P < 0.0001$.

to sustain obesity. Consistent with a previous report (*42*), we noticed a slight trend toward decreased expression of *FAS*, *SCD1*, and *ACLY* lipogenic genes in gWAT from B7-H3 KO obese mice as compared to WT lean mice (fig. S9F). Furthermore, similar to young mice before obesity onset (Fig. 7D), gWAT from B7-H3 KO obese mice showed decreased OCR as compared to WT depot (Fig. 8L), while liver and BAT OCRs were similar (fig. S9, G and H), confirming reduced oxidative metabolism in B7-H3 KO adipose tissue.

During obesity, when the ability of adipose tissue to store and sequester lipids is compromised, excess of lipids can begin to ectopically accumulate in organs such as the liver. Consistent with this notion, we observed that livers were considerably heavier in B7-H3 KO female (Fig. 8M) and male mice (Fig. 8N). Furthermore, hematoxylin and eosin (H&E) staining of liver sections revealed TG accumulation in the livers of B7-H3 KO male mice (Fig. 8O), a condition known as macrovesicular hepatic steatosis, which is a common occurrence during obesity and insulin resistance. In summary, our results show that B7-H3 deficiency induces obesity-associated systemic metabolic deregulation.

Adipose tissue from B7-H3 KO mice display early and late inflammation that is worsened by HFD

Because obesity is classically associated with chronic low-grade adipose tissue inflammation (*43*), we sought to test whether B7-H3 KO mice exhibit adipose tissue inflammation. To this end, we analyzed major immune cell types residing in the gWAT of WT and B7-H3 KO mice fed a regular chow diet, using flow cytometry at an early age before obesity onset and at a later time point. At 6 weeks old, i.e., before the body weight divergence between WT and KO mice, we found that $CD45^+$ immune cell frequency was increased in KO gWAT (Fig. 9A), but the cell number per gram of fat was similar (fig. S10A). We found elevated numbers of adipose neutrophils in B7-H3 KO mice fed a regular diet (Fig. 9B). Neutrophils have been shown to infiltrate the adipose tissue very early after HFD feeding and to suppress insulin signaling (*44*). Neutrophil depletion through antibody treatment did not prevent obesity development in B7-H3 KO mice (fig. S10B), suggesting that neutrophil recruitment is not essential to obesity onset in KO mice. Eosinophils, type 2 innate lymphoid cells (ILC2), and NKT cells are innate immune cells known to maintain immune and metabolic homeostasis of the adipose tissue through secretion of anti-inflammatory cytokines and maintenance of tissue-resident M2 macrophages (*45*). We found that these three populations were decreased in the B7-H3 KO tissue (Fig. 9C), indicating early loss of immune homeostasis before body weight divergence between WT and KO mice. At 16 weeks of age, during obesity, both $CD45^+$ immune cell frequency (fig. S10C) and absolute number (Fig. 9D) were significantly elevated in B7-H3 KO animals. Similar to early stage, proportions of eosinophils, ILC2, and NKT cells remained lower in the KO compared to WT mice (fig. S10D). We observed a trend toward an increased infiltration of total macrophages and T cells in B7-H3 KO fat (fig. S10E). Adipose regulatory T cells (T_{regs}) were also unexpectedly elevated in B7-H3 KO mice (fig. S10E), likely as a regulatory response to the excessive local inflammation. In adipose tissue, the expression of CD11c and CD206 markers distinguishes proinflammatory M1 from regulatory M2 macrophages, respectively (*46*). We observed an increased frequency of M1 subtype and decreased frequency of M2 subtype among the total pool of macrophages in the B7-H3 KO gWAT (Fig. 9E), resulting in higher M1/M2 ratio (Fig. 9F). Moreover, M1 macrophage absolute cell numbers were significantly elevated in KO tissue (Fig. 9G), confirming that, during obesity, B7-H3–deficient mice develop substantial inflammation in fat tissue.

To investigate whether excessive fat intake further worsens adipose tissue inflammation in B7-H3–deficient animals, we fed WT and B7-H3 KO mice with a HFD (60% fat) and analyzed immune cell infiltration in gWAT. First, we confirmed that the proportion (fig. S10F) and total number of immune cells (Fig. 9H) were higher in the B7-H3 KO gWAT compared to WT tissue. Moreover, we found that HFD feeding exacerbated the immune cell infiltration in gWAT from B7-H3 KO mice compared to a regular chow (Fig. 9, D and H). gWAT from B7-H3 KO mice contained about six times more macrophages than gWATs from WT controls (Fig. 9I), with M1 proinflammatory cells accounting for half of the total macrophages in B7-H3 KO tissue (Fig. 9J). We observed that proportions of eosinophils, ILC2, and NKT cells were decreased (fig. S10G), while numbers of mast cells, inflammatory monocytes, dendritic cells, and T cells were significantly elevated in gWAT from B7-H3 KO mice as compared to WT controls (Fig. 9K). Overall, we found that adipose tissue inflammation significantly worsens with HFD feeding in B7-H3 KO mice. Together, our data suggest that metabolic deregulations in B7-H3 KO mice are associated with early proinflammatory signals in adipose tissue, which evolve into a more chronic obesity-associated inflammation over time.

DISCUSSION

Immune checkpoints play key roles in the regulation of cellular immunity (*47*), as they are essential for maintaining immune homeostasis and preventing autoimmunity. Moreover, tumors exploit these immune modulatory pathways to suppress and evade immune clearance. In this context, the immune checkpoint B7-H3 has been mostly studied for its role in the tumor microenvironment and as a promising target for cancer immunotherapies (*2*). However, little is known about tissue expression and potential nonimmune function of B7-H3. In this study, we reveal an unexpected metabolic role for B7-H3 in adipose tissue. We showed that B7-H3 is highly expressed in mouse and human APs and dysregulated with obesity. B7-H3 may not only serve as a previously unrecognized marker of APs but also stimulated their glycolytic and oxidative metabolism. Moreover, adipocytes differentiated from B7-H3–deficient APs were less oxidative and stored more fat. Consequently, B7-H3 KO mice rapidly developed spontaneous obesity on a normal chow diet. The rapid weight gain was accompanied by a strong accumulation of WAT containing hypertrophic adipocytes. The B7-H3 KO mice exhibited hyperglycemia, hyperinsulinemia, dyslipidemia, liver steatosis, and decreased WAT lipolysis and FA oxidation. Furthermore, we demonstrated that obesity in B7-H3 KO mice was associated with marked adipose tissue inflammation.

Recent studies reported a link between immune checkpoint and cellular metabolism in cancer (*48*). For example, blocking PD-L1 on tumors dampens glycolysis by inhibiting mTOR activity (*49*). Likewise, B7-H3 promotes aerobic glycolysis in cancer cells (*3*, *50*) by regulating the glycolytic enzyme HK2 (*4*). In addition, c-myc may be involved in the downstream pathway of B7-H3–regulated glycolysis in HeLa cells (*50*). In line with these studies, our RNA-seq analysis showed that c-myc and its target genes, such as HK2, were downregulated in B7-H3 KO APs. Our work highlights that constitutive expression of B7-H3 allows for metabolic regulation in nonmalignant

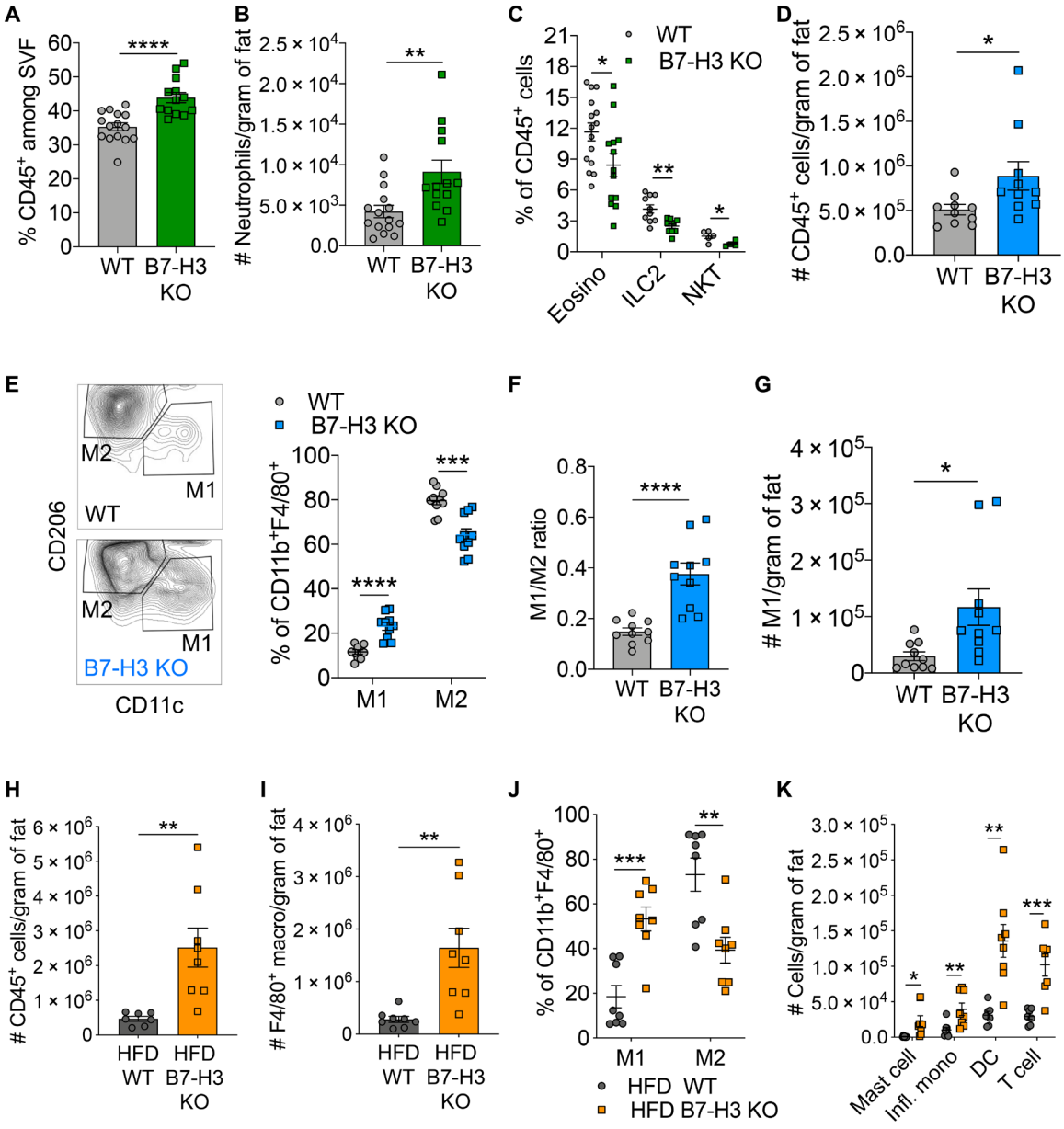

Fig. 9. B7-H3 KO mice exhibit early and late adipose tissue inflammation. (**A** to **C**) Immune cell populations of gWAT from 6-week-old WT ($n = 15$) and B7-H3 KO ($n = 15$) mice fed a regular chow diet were analyzed by flow cytometry. (A) Proportion of $CD45^+$ immune cell among total SVF. (B) Number of neutrophils per gram of fat. (C) Proportion of anti-inflammatory type 2 immune cell subsets among total $CD45^+$ immune cells. (**D** to **G**) Immune cell populations of gWAT from 5-month-old WT ($n = 10$) and B7-H3 KO ($n = 10$) mice fed a regular chow diet were analyzed by flow cytometry. (D) Number of $CD45^+$ cells per gram of fat. (E) Representative dot plots and proportions of $CD11c^+$ M1 proinflammatory and $CD206^+$ M2 tissue-resident macrophages among total $CD11b^+F4/80^+$ macrophages. (F) Ratio of M1 over M2 macrophages. (G) Absolute number of $CD11c^+F4/80^+$ M1 macrophages per gram of fat. (**H** to **K**) WT ($n = 10$) and B7-H3 KO ($n = 10$) mice were fed with a HFD for 14 weeks before analysis of immune cell infiltration in gWAT. (H) Absolute number of $CD45^+$ immune cell per gram of fat. (I) Absolute number of $F4/80^+$ macrophages per gram of fat. (J) Proportion of M1 and M2 macrophages among total macrophages. (K) Absolute number of various proinflammatory immune cell subsets per gram of fat. Data are represented as means ± SEM between two (D to K) to three (A to C) independent experiments. Data were analyzed by Student's *t* test. $^*P < 0.05$, $^{**}P < 0.01$, $^{***}P < 0.001$, and $^{****}P < 0.0001$. DC, dendritic cell. Eosino, eosinophil; Infl. mono, inflammatory monocyte.

progenitor cells. Thus, it appears that cancer cells may exploit this intrinsic metabolic pathway by overexpressing B7-H3 to reprogram their glucose metabolism and support tumor growth (*3*). Consistent with this idea, cancer cells and stem cells have been shown to share common metabolic signatures (*51*).

We found that B7-H3 expression was gradually decreased in developing adipose tissue through embryonic and postnatal stages and during preadipocyte differentiation into adipocytes. In contrast, B7-H3 is highly expressed in developing bones during embryogenesis, and its expression increases as osteoblast precursor

cells differentiate into mature osteoblasts, thereby promoting bone mineralization (*52*). Glycolysis seems to be an essential feature of osteoblast differentiation, whereas differentiated adipocytes prefer oxidative phosphorylation (*53*). As we showed that B7-H3 promoted glycolysis, this explains the differences in expression during lineage specification and how B7-H3–dependent metabolic programming influences cell fate and the degree of bone formation and adiposity. By promoting glycolysis, B7-H3 may contribute to maintain stemness (*26*). Thus, down-regulation of B7-H3 during adipocyte differentiation may allow metabolic reprogramming toward the adipocyte lineage (*28*). Similar to B7-H3 KO mice, Thy1 (CD90) KO mice have increased body fat and decreased bone mass (*54*). Thy1 promotes osteogenesis but inhibits adipogenesis of mesenchymal stem cells. Recent studies have shown that B7-H3 knockdown induces differentiation of human glioblastoma by modulating myc expression (*55*) and angiogenic differentiation of human late endothelial progenitor cells (*56*). In our study, while we saw no effect of B7-H3 on adipocyte differentiation per se, adipocytes derived from B7-H3–deficient APs had a reduced oxidative metabolism and accumulated more lipids. In a recent human study, molecularly distinct human AP subtypes differentiate into adipocytes with different metabolic capacities (*57*). Further studies are warranted to understand how B7-H3 expression in progenitors drives a particular metabolic program in the adipocyte progeny.

Metabolic changes in APs modify nutrient availability and metabolite secretion into the adipose microenvironment, thereby affecting cellular metabolism and function of neighbor cells. By performing Seahorse analysis, we demonstrated that the lack of B7-H3 in APs reduced lactate production, which was associated with decreased lipid oxidation in whole fat depot. Lactate has recently emerged as an important metabolic substrate feeding the oxidative metabolism of adipocytes (*58*). Therefore, decreased lactate secretion by B7-H3 KO APs could impair the metabolism of surrounding adipocytes. Besides metabolites, our RNA-seq analysis also identified changes in inflammatory response, chemokines, and cytokine secretion by B7-H3 KO APs. We observed that IL-6 was down-regulated in B7-H3 KO APs. A large body of literature supports the notion that IL-6 plays an essential physiological role in the regulation of adipose tissue and lipid metabolism (*59*). IL-6 KO mice develop mature-onset obesity (*60*). Moreover, IL-6 promotes lipolysis and β-oxidation in adipocytes (*61*). Further experiments will be needed to explore the potential contribution of the B7-H3/IL-6 pathway in metabolic homeostasis.

One major finding of our study is that B7-H3 KO mice develop spontaneous obesity on a normal chow diet. The lack of B7-H3 did not alter food intake and activity as usually seen in other murine obesity models (*22*). Instead, we reveal that B7-H3 promotes lipolysis and FA oxidation in adipocytes, thereby limiting excessive lipid storage. Last, it is unexpected that the immunoregulatory function of B7-H3, notably on T cells, does not play a role in obesity development. Instead, our data indicate that adipose tissue inflammation develop as a consequence of early metabolic dysfunction but likely contributes to insulin resistance later on.

In summary, we show that B7-H3, an immune checkpoint that has been widely studied in the tumor microenvironment and is a target of cancer immunotherapy in clinical trials, is predominantly expressed on APs and controls AP metabolism, as well as the lipolytic and oxidative properties of differentiated adipocytes, therefore limiting lipid storage and protecting from obesity. The B7-H3 pathway might offer a new therapeutic avenue to explore new treatment of obesity and metabolic diseases, which remains a medicinal challenge (*62*). For example, modulating the B7-H3 pathway through the use of agonistic antibodies might constitute a novel pharmacologic approach for weight loss management. Future studies are warranted to explore the feasibility, efficacy, and safety of these approaches.

Limitations of the study

B7-H3 was originally described as a ligand binding to its unknown receptor on T cells (*63*). Some recent studies suggest that it can function as a receptor, but potential ligands and mechanisms of signal transduction remain unknown. In this study, we did not address whether B7-H3 acted as a ligand and/or receptor to regulate AP metabolism. The B7-H3 intracytoplasmic domain, which lacks canonical signaling motifs, was recently shown to bind to the major vault protein (MVP), thus activating the mitogen-activated protein kinase pathway and promoting cancer cell stemness (*64*). MVP gene knockout aggravates HFD-induced obesity in mice (*65*). Further investigations will be needed to evaluate the potential role of MVP in B7-H3 signaling in APs. Furthermore, we did not address the consequences of increased B7-H3 levels found in the tissue from obese participants because of the difficulties of testing this in human individuals and in murine models overexpressing B7-H3. Our results tempt us to speculate that this up-regulation is protective, although future studies will be required to validate this hypothesis.

MATERIALS AND METHODS

Animals and animal care

B7-H3 KO mice were previously generated (*66*) and had been backcrossed at least 12 generations onto the C57Bl/6 background. B7-H3 KO mice were crossed to Rag1 KO mice (Jackson Laboratory). Double Rag1.B7-H3 KO mice were used for experiments and compared to Rag1 littermate controls. C57Bl/6 WT control mice and MyD88$^{-/-}$ mice were purchased from Jackson Laboratory. B7-H3$^{+/+}$ control littermates were generated by backcrossing B7-H3 KO mice to C57Bl/6 WT mice. PD-L1$^{-/-}$ mice were previously reported (*67*).

All mice were housed and bred within a pathogen-free barrier facility that maintained a 12-hour light/12-hour dark cycle, at 20° to 22°C. Experiments were conducted on female mice unless otherwise stated. Mice were fed a normal chow diet (PicoLab Mouse Diet 20; 5058, LabDiet) and had access to sterile water ad libitum. Alternatively, mice were fed with a low-fat diet (PicoLab Mouse Diet 20; 5053, LabDiet) or HFD (58Y1 60% kcal % of fat, TestDiet). From 5 weeks old until 30 weeks old, mice were monitored for body weight. All animal studies were in compliance with the National Institutes of Health Guide for the Care and Use of Laboratory Animals and were approved by the Institutional Animal Care and Use Committee at Albert Einstein College of Medicine.

ITT and GTT

For ITT, mice were fasted for 5 hours. Recombinant insulin (0.5 U/kg of lean mass) was injected intraperitoneally, and blood glucose concentrations were measured before and 30, 60, and 120 min after insulin injection with the OneTouch Glucose Monitoring System (LifeScan Inc.). For GTT, mice were fasted for 12 hours. IPGTT was performed following an intraperitoneal injection of glucose (1 g/kg of lean mass). Blood glucose levels were analyzed before and 30, 60, and 120 min following glucose injection. For OGTT, glucose was

administered by gavage, and both blood glucose and insulin levels were measured before and 30, 60, and 120 min after gavage. Insulin was measured with the Ultra-Sensitive Mouse Insulin ELISA Kit (Crystal Chem Inc.).

Histology and IHC

Mouse tissues were collected, fixed with 10% neutral buffer formalin, and embedded in paraffin. Tissue sections were cut and stained with H&E. H&E-stained tissues were imaged with a slide scanner microscope. To measure adipocyte hypertrophy, the cross-sectional size (area; μm^2) of adipocytes (100 cells per mouse) was determined in gWAT using Adiposoft plug-in in ImageJ software.

Human subcutaneous fat tissue was obtained from obese participants (BMI over 35 to 55 kg/m^2, aged 18 to 65 years) undergoing gastric bypass surgery. Samples were collected in the context of clinical care during the patient's routine gastric bypass operation. Adipose tissue was only collected at baseline during the surgery. Participants were excluded if they were taking anti-inflammatory and/or immunosuppressive drugs, currently smoked, or had been diagnosed with significant gastrointestinal disease or inflammatory bowel disease. Study participants were enrolled in accordance with the Helsinki Declaration and provided written informed consent. The study was approved by the Gothenburg Ethical Review Board #682-14 (ClinicalTrials.gov, NCT02322073). Human fat tissue was fixed in Histofix solution (Histolab, #1000) and embedded in paraffin. After antigen retrieval using 1× citrate unmasking solution (Cell Signaling Technology (B7-H3) , #14746), slides were stained with rabbit anti-CD276 (B7-H3) monoclonal antibody (mAb) (Cell Signaling Technology, D9M2L) and the SignalStain Boost IHC Detection Reagent (HRP, Rabbit; #8114) following the manufacturer's instructions. Slides were imaged with a slide scanner microscope.

Flow cytometry

Purified cells were first incubated with Fc block (Tonbo) and live-dead marker in 1× phosphate-buffered saline (PBS)/2 mM EDTA/2% fetal bovine serum (FBS)/0.1% azide FACS buffer for 20 min at 4°C. Primary antibodies were then added for 30 min at 4°C. Cells were washed twice with FACS buffer and incubated with secondary antibodies. For intracellular staining, cells were fixed and permeabilized using a commercial kit (eBioscience) per the manufacturer's instructions. Briefly, fixation/permeabilization buffer was added to the cells for 20 min at room temperature (RT). Cells were washed with permeabilization buffer and incubated with primary intracellular antibody for 30 min at 4°C or overnight. After two washing steps, cells were resuspended in FACS buffer and were ready for acquisition. Several antibody cocktails were used to identify distinct cell populations within mouse adipose depots. Immune cells are $CD31^-CD45^+$. Endothelial cells are $CD45^-CD31^+$. Total macrophages are identified as $CD31^-CD45^+CD11b^+F4/80^+$. Proinflammatory M1 macrophages are $CD31^-CD45^+CD11b^+F4/80^+CD11c^+$. Tissue-resident M2 macrophages are $CD31^-CD45^+CD11b^+F4/80^+CD206^+$. Dendritic cells are $CD31^-CD45^+CD11b^+CD11c^+$. Neutrophils are $CD31^-CD45^+CD11b^+Ly6G^+$. Eosinophils are $CD31^-CD45^+CD11b^+SiglecF^+$. Monocytes are $CD31^-CD45^+CD11b^+Ly6G^-Ly6C^+$. T cells are $CD31^-CD45^+CD3^+$. T_{regs} are $CD31^-CD45^+CD3^+CD4^+FoxP3^+$. B cells are $CD31^-CD45^+B220^+$. NK cells are $CD31^-CD45^+NK1.1^+$. NKT cells are $CD31^-CD45^+CD3^+NK1.1^+$. ILC2 cells are $CD31^-CD45^+Lin^-$ ($CD11c^-CD11b^-F4/80^-SiglecF^-CD3^-B220^-$) $GATA3^+IL\text{-}33R^+$. Mast cells are $CD31^-CD45^+FceRI\alpha^+$. For progenitor/stem cell staining, anti-CD45, CD31, CD29, CD90, Sca1, PDGFRα, CD34, and CD24 mAbs were used. Mouse B7-H3 was stained with BAF1397 anti-mouse B7-H3–biotin (R&D Systems), followed by streptavidin conjugated to a fluorochrome. The BAF108 normal goat IgG-biotin was used as isotype control (R&D Systems). Data were acquired using a BD LSRII flow cytometer (BD Biosciences) and analyzed using FlowJo software (version 10).

Neutrophil depletion

Five-week-old B7-H3 KO mice were injected intraperitoneally with 100 μg of InVivoPlus anti-mouse Ly6G (clone 1A8, Bio X Cell) twice a week for 8 weeks. Depletion was confirmed by flow cytometry in mouse peripheral blood mononuclear cells.

Analysis of body composition, food intake, and locomotor activity

Animals were analyzed for body composition by quantitative NMR imaging and CT scan. Mice were single-housed for a week before food intake measurement. Food was weighed daily for 4 days, and daily average food consumption was calculated. For detailed food intake study (meal number, size, interval, duration, and satiety ratio), mice were single-housed in a metabolic chamber (Oxymax CLAMS System, Columbus Instruments). After 3 days of acclimatation, detailed patterns of food intake were recorded, analyzed, and averaged over 3 days. Similarly, energy expenditure and spontaneous locomotor activity were recorded and analyzed in acclimated mice single-housed for 3 days in metabolic chambers. Energy expenditure data were analyzed using CalR, a web-based analysis tool (https://calrapp.org/) (*68*).

Total RNA extraction and quantitative reverse transcription polymerase chain reaction analysis

Total RNA was extracted from total gWAT, iWAT, and BAT using the RNeasy Lipid Tissue Mini Kit (QIAGEN) following the manufacturer's instructions. Total RNA was extracted from freshly isolated gWAT SVF using the RNeasy Plus Micro Kit (QIAGEN) following the manufacturer's instructions. For primary adipocytes, the RNeasy Lipid Tissue Mini Kit (QIAGEN) was used with slight modifications. Briefly, freshly isolated adipocytes were lysed in TRIzol LS by vortexing for 30 s. The homogenate was then incubated 5 min at 37°C in a water bath to liquefy the lipids and centrifuged at 3200*g* for 15 min at RT. The lower aqueous phase was secured into a syringe and transferred into a new tube, while the top layer (lipids) was discarded. Further steps followed the manufacturer's protocol starting back with adding chloroform to the aqueous phase. Genomic DNA was removed using the RNase-Free DNase Set (QIAGEN). Total RNA was extracted from ex vivo–expanded APs using the RNeasy Plus Micro Kit (QIAGEN) following the manufacturer's instructions. Total RNA was extracted from ex vivo–differentiated adipocytes using the RNeasy Plus Micro Kit (QIAGEN) with modifications. Cells were lysed in QIAzol by homogenization with a 1-ml syringe and 23-gauge needle. The homogenate was then incubated 5 min at 37°C in a water bath to liquefy the lipids and centrifuged at maximum speed for 15 min at RT. The lower aqueous phase was secured into a syringe and transferred into a new tube, while the top layer (lipids) was discarded. Chloroform (200 μl) was added, and the tube was shaken for 15 s and incubated at RT for 3 min. The mixture was centrifuged at 12,000*g* for 15 min at 4°C, and the upper aqueous phase was transferred into a new tube. Further steps

followed the RNeasy Plus Micro Kit (QIAGEN) manufacturer's protocol starting back with adding 70% ethanol to the aqueous phase.

For TaqMan-based quantitative real time polymerase chain reaction (qRT-PCR), complementary DNA (cDNA) was synthesized using the SuperScript VILO cDNA Synthesis Kit (Thermo Fisher Scientific). Gene expression was assessed by TaqMan Technology using The TaqMan Gene Expression Master Mix (Thermo Fisher Scientific) with specific probes (listed in Table 1 oligonucleotides) and ABI 7900 qRT-PCR or ViiA 7 Real-Time PCR machines.

For the RT^2 Profiler PCR array mouse mitochondrial energy metabolism (QIAGEN; SybR Green-based qRT-PCR), cDNA was synthesized using the RT^2 First Strand Kit (QIAGEN). Data were analyzed using the web-based RT^2 Profiler PCR Array data analysis software (https://geneglobe.qiagen.com/us/analyze).

ORO staining and quantification

ORO working solution was freshly prepared each time by mixing 3 parts of stock ORO (in 100% isopropanol) with 2 parts of dH_2O. The mixture was filtered on 0.22 μm after 20 min and used within 2 hours. Cells were washed twice with PBS, fixed with 4% paraformaldehyde for 30 min and washed twice with dH_2O. After a 5-min incubation with 60% isopropanol, cells were stained with ORO for 20 min on a rocker shaker, washed five times with dH_2O, counterstained with hematoxylin for 1 min, and washed three times with dH_2O. Images were taken under bright light with an EVOS microscope. To quantify intracellular ORO, 100% isopropanol was added to the well for 15 min on a rocker shaker to dissolve ORO. The absorbance was measured at 510 nm using a Synergy H4 hybrid reader (BioTek).

HCS LipidTOX staining

Isolated APs were grown and differentiated into adipocytes on glass coverslips in 24-well plates. Cells were fixed with 3% paraformaldehyde in 1× PBS for 30 min at RT, followed by three washes with 1× PBS. Cells were stained with 100 μl of 1× HCS LipidTOX Red neutral lipid stain in 1× PBS (Thermo Fisher Scientific; 200× stock solution) for 1 hour at RT, followed by two washes with 1× PBS. Cells were counterstained with the ProLong Gold Antifade Mountant with 4′,6-diamidino-2-phenylindole (DAPI), let dry overnight at RT in the dark, and stored at 4°C in the dark until imaging with a Leica SP8 confocal microscope.

Generation of BM chimeras

Six-week-old recipient mice were sublethally irradiated at 1200 rads with a cesium-source irradiator. Irradiated mice were treated with antibiotics (sulfamethoxazole and trimethoprim, Hi-Tech Pharmacal) in drinking water for 2 weeks to prevent infections. Bones were harvested from donor mouse, cut at both ends, and placed into a 0.5-ml tube pierced at the bottom. This tube was nested in a 1.5-ml microcentrifuge tube and centrifuged 10,000*g* for 2 min at 4°C to spin out the BM from the bones. One milliliter of RPMI and 10% FBS and 2 mM EDTA were added to the cells. The cell suspension was filtered on 70 μm mesh, counted, washed twice with PBS, and filtered on 40 μm before injection. Cells (2.5×10^6) in 200 μl of PBS were administered to irradiated recipients via retro-orbital injection.

Isolation of SVF and differentiation

Mice gWAT or iWAT were harvested in Hanks' balanced salt solution (HBSS) 0.5% bovine serum albumin (BSA), minced, and incubated with collagenase II (2 mg/ml) and 5 mM $CaCl_2$ for 20 to 45 min at 37°C on a rotational shaker. Ten milliliters of HBSS, 0.5% BSA, and 2 mM EDTA were added to stop the digestion. The homogenate was filtered onto 300 μm mesh and centrifuged at 150*g* for 8 min at RT. Floating adipocytes on top were collected, transferred to a new tube, washed, and ready for analysis. The pellet, containing SVF cells, was washed and centrifuged at 500*g* for 10 min at 4°C. For flow cytometry analysis, erythrocytes were lysed using 2 ml of red blood cell lysis buffer (Tonbo) for 5 min at RT. The SVF cell suspension was washed, filtered on a 70 μm strainer, and stained with specific antibody cocktails. For AP isolation, the adipose tissue progenitor isolation kit (Miltenyi) was used according to the manufacturer's instructions. Isolated cells were plated for expansion in Dulbecco's modified Eagle's medium (DMEM) (Corning, 10-0170CV) containing high glucose and pyruvate, supplemented with 10% FBS and 1% penicillin (pen)/streptomycin (strep). Cells were grown to confluence. Two days after confluency, adipogenic differentiation cocktail composed of 1 μM dexamethasone, insulin (5 μg/ml), 0.5 mM 3-isobutyl-1-methylxanthine (IBMX), and 1 μM rosiglitazone was added for 2 days. Differentiated cells were then maintained in enriched DMEM with insulin (5 μg/ml).

ECAR and OCR measurements

Cells

Cell bioenergetics was determined using the Extracellular Flux Analyzer (XF24; Seahorse Biosciences). APs were seeded in an XF24-well microplate at 20,000 cells per well 1 day before the assay. The sensor cartridge was hydrated in a Seahorse XF calibrant overnight. Glycolytic activity was analyzed with the Glycolysis Stress Test Kit. Cells were incubated in Seahorse XF base medium supplemented with 2 mM glutamine for 1 hour at 37°C in a CO_2-free incubator. Both ECAR and OCR were recorded over time before and after sequential injection of the following compounds: (i) glucose (10 mM), (ii) oligomycin (1 μM), and (iii) 2-deoxyglucose (50 mM). Each measurement cycle consisted of 3 min of mixing, 2 min of waiting, and 3 min of recording.

Tissues

Tissue bioenergetics was determined as previously described (*69*). Briefly, BAT, WAT, and liver were collected rapidly after euthanasia and rinsed with Krebs-Henseleit buffer (KHB) (111 mM NaCl, 4.7 mM KCl, 2 mM $MgSO_4$, 1.2 mM Na_2HPO_4, 0.5 mM carnitine, 2.5 mM glucose, and 10 mM sodium pyruvate). Tissues were cut into small pieces (8 to 13 mg) and quickly transferred to individual wells of an XF24 plate. Individual pieces were stabilized from excessive movement by islet capture screens (Seahorse Bioscience), and 675 μl of KHB (supplemented with 2 mM ATP, 0.5 mM CoA, 0.1 mM NAD, and 2 mM sodium pyruvate) was added to each well. Digitonin was added to enhance plasma membrane permeability. Basal OCR was determined at 37°C according to the following plan: Basal readings were recorded every 2 min for five readings, followed by exposure to digitonin. Subsequent readings were recorded after 2 min of mixing and 2 min of rest. Basal OCR values were normalized to individual tissue weights.

Mitochondria staining

Isolated APs were stained with 100 nM MitoTracker Green FM (Invitrogen) and 10 nM MitoTracker Deep Red (Invitrogen) in 1× PBS with 2% FBS for 15 min at 37°C, followed by two washes in 1× PBS with 2% FBS. Data were acquired using BD FACSCalibur (BD Biosciences) and analyzed using FlowJo software (version 10).

Table 1. Oligonucleotide primers listed 5′ to 3′ ends.

#	Name	Primer sequence
1	B7-H3 sgRNA 1 (forward)	CACCGAAAAAGTCCGCGATTACGTC
2	B7-H3 sgRNA 1 (reverse)	AAACGACGTAATCGCGGACTTTTTC
3	B7-H3 sgRNA 2 (forward)	CACCGAAAACGGCTCGATCGGTGAT
4	B7-H3 sgRNA 2 (reverse)	AAACATCACCGATCGAGCCGTTTTC
5	Scramble 1 (forward)	CACCGAAAAAGTCCGCGATTACGTC
6	Scramble 1 (reverse)	AAACGACGTAATCGCGGACTTTTTC
7	Scramble 2 (forward)	CACCGAAAACGGCTCGATCGGTGAT
8	Scramble 2 (reverse)	AAACATCACCGATCGAGCCGTTTTC
9	Not I B7-H3	CCATTTCAGGTGTCGTGAGCGGCCGCATGCTTCGAGGATGGGGTG
10	Hpa I B7-H3	CCGGGTACTCTAGAATAGTTAACTCAAGCAATTTCTTGTCCGTC
11	TaqMan probe mB7-H3	Mm00506020_m1
12	TaqMan probe leptin	Mm00434759_m1
13	TaqMan probe adiponectin	Mm00456425_m1
14	TaqMan probe FAS	Mm00662319_m1
15	TaqMan probe SCD1	Mm00772290_m1
16	TaqMan probe ACLY	Mm01302282_m1
17	TaqMan probe SREBP1	Mm00550338_m1
18	TaqMan probe ChREBP	Mm02342723_m1
19	TaqMan probe LPL	Mm00434764_m1
20	TaqMan probe PEPCK	Mm00551411_m1
21	TaqMan probe PAT2	Mm00462617_m1
22	TaqMan probe TMEM26	Mm01173641_m1
23	TaqMan probe PRDM16	Mm00712556_m1
24	TaqMan probe UCP1	Mm01244861_m1
25	TaqMan probe P2RX5	Mm00462617_m1
26	TaqMan probe FATP	Mm00449511_m1
27	TaqMan probe CD36	Mm00432403_m1
28	TaqMan probe GAPDH	Mm99999915_g1
29	TaqMan probe TBP	Mm01277042_m1
30	TaqMan probe PDGFRα	Mm00440701_m1
31	TaqMan probe LY6A (Sca1)	Mm00726565_s1
32	TaqMan probe PPARγ	Mm00440940_m1
33	TaqMan probe CEBPα	Mm00514283_s1
34	TaqMan probe FABP4	Mm00445878_m1
35	TaqMan probe SLC2A4 (Glut4)	Mm00436615_m1
36	TaqMan probe PLIN1	Mm00558672_m1
37	TaqMan probe PLIN3	Mm04208646_g1
38	TaqMan probe HK2	Mm00443385_m1
39	TaqMan probe CPT1A	Mm00550448_m1
40	TaqMan probe HADHA	Mm00805228_m1

Intracellular ROS staining

SVF was stained with 1 μM CellROX Green Reagent (Invitrogen) in DMEM for 30 min at 37°C, followed by two washes in 1× PBS and staining with an antibody cocktail for APs. Data were acquired using a BD LSRII flow cytometer (BD Biosciences) and analyzed using FlowJo software (version 10).

In vitro FA uptake assay

Isolated APs were plated in a flat-bottom 96-well plate at 5×10^5 cells per well in 200 μl of DMEM supplemented with glucose, pyruvate, 10% FBS, and 1% pen/strep. Two days after the cells reached confluence, differentiation was induced with an adipogenic cocktail containing 1 μM dexamethasone, insulin (5 μg/ml), 0.5 mM IBMX, and 1 μM rosiglitazone for 3 days. Cells were then maintained in culture medium containing insulin (5 μg/ml) for 2 days. On day 6, insulin was removed. The assay was performed on day 7 using the QBT Fatty Acid Uptake Assay Kit (Molecular Devices) per the manufacturer's instructions. Briefly, cells were first serum-starved for 2 hours and then treated with 50 nM insulin for 1 hour. The kit loading buffer, containing the BODIPY dodecanoic acid fluorescent FA analog, was added to the cells, and fluorescence was immediately recorded every minute for 60 min using a bottom-read mode microplate reader.

TG absorption assay

Overnight-fasted mice were administered a corn oil gavage [20 × body weight (μl)]. Blood samples were obtained by retro-orbital bleeding at 0, 1, 2, and 6 hours after the corn oil gavage and serum TG levels were determined using a commercial kit and following the manufacturer's instructions (Free Glycerol Reagent, Sigma-Aldrich, F6428; Triglyceride Reagent, Sigma-Aldrich, T2449).

Cell culture and differentiation

hADSCs were purchased from Lonza. 3T3-L1 cells were purchased from ZenBio and used at low passage. Ing-svf cells were a gift from R. Gupta (*24*). Low-passage cells were cultured in DMEM (Corning, 10-0170CV) containing high glucose and pyruvate, supplemented with 10% FBS, 1% pen/strep at 37°C, and 10% CO_2. Cells were grown to confluence. Two days after confluency, adipogenic differentiation cocktail was added for 2 days: 0.25 μM dexamethasone, insulin (1 μg/ml), 0.5 mM IBMX, and 2 μM rosiglitazone for 3T3-L1 cells and 1 μM dexamethasone, insulin (5 μg/ml), 0.5 mM IBMX, and 1 μM rosiglitazone for Ing-svf cells. Differentiated cells were then maintained in enriched DMEM with insulin (2 μg/ml) or insulin (5 μg/ml) for 3T3-L1 and Ing-svg, respectively.

Western blotting

Cell pellets were incubated with ice-cold radioimmunoprecipitation assay (RIPA) lysis buffer with proteinase inhibitor cocktail [Protease and Phosphatase Inhibitor cocktail (100×), Thermo Fisher Scientific] for 30 min at 4°C on a rotational shaker. The cell lysate was centrifuged for 20 min 13,000*g* at 4°C, and the supernatant containing proteins was aliquoted and stored at −20°C. Protein concentration was determined using the Pierce BCA protein Assay Kit (Thermo Fisher Scientific). Each sample was mixed with Laemmli buffer (Bio-Rad) and boiled at 100°C for 5 min to denature proteins. Samples were loaded onto an ExpressPlus PAGE 12% gel (GenScript) and run for 45 min at 140 V in tris-MOPS-SDS running buffer. The Mini-Trans-Blot Electrophoretic Transfer Cell System (Bio-Rad) was used to transfer the proteins onto a polyvinylidene difluoride membrane per the manufacturer's instructions. The membrane was first blocked with 5% milk TBST (Tris-buffered saline with 0.1% Tween® 20) for 1 hour at RT followed by overnight incubation with primary antibody diluted in 2% milk TBST at 4°C. The membrane was washed several times with TBST, incubated with secondary antibody for 1 hour at RT, and washed again. Clarity Western ECL substrate (Bio-Rad) reagent was used for signal development and a Bio-Rad detection machine. The following antibodies were used for Western blot: anti–B7-H3 (AF1397, R&D Systems), anti-actin (C11, Santa Cruz Biotechnology), anti-goat horseradish peroxidase (HRP) (catalog no. 805-035-180), anti-Plin1 (D418, Cell Signaling Technology), and anti-rabbit HRP (7074, Cell Signaling Technology).

Metabolic measurements

Blood was collected after an overnight fasting. Glucose, total cholesterol, TGs, nonesterified free FAs, insulin, and leptin concentrations were determined in blood serum at the Biomarker Analytic Research Core at Albert Einstein College of Medicine.

RNA-seq and pathway analysis

Six age- and weight-matched B7-H3 KO mice and six WT control mice fed a 10% fat-purified diet (58Y2, TestDiet) were used at 10 weeks old. Three gWATs were pooled into one sample and processed as described above. Single-cell suspension was incubated with Fc block, CD31, CD45, PDGFRα, Sca1, and B7-H3 antibodies at 4°C for 20 min, washed, and incubated with streptavidin for another 20 min at 4°C. Cells were filtered on 40 μM, and DAPI was added. A total of 7.10^4 to 2.10^5 B7-H3 KO and WT APs were sorted with a FACSAria cell sorter and immediately processed for RNA extraction using an RNeasy Micro Plus kit (QIAGEN). RNA integrity and concentration were evaluated with the Bioanalyzer High Sensitivity Chip (Agilent). High-quality total RNA (RNA integrity number > 8.0) was used to generate directional RNA-seq libraries using the KAPA RNA HyperPrep Kit with RiboErase Kit (KK8560). Seventy-five–base pair, single-end sequencing was performed on the Illumina NextSeq 500 platform at the Epigenomics Shared Facility (Albert Einstein College of Medicine) to a depth of at least 30 million reads per sample. Read alignment to the mouse genome (mm10) and read counts to genes were generated using the STAR software (https://github.com/alexdobin/STAR) (*70*) with –quantmode. EdgeR (version 3.10) (*71*) was used to compute the gene expression difference between WT and B7-H3 KO samples. A fold change of ≥2 and adjusted *P* value of ≤0.05 were set as cutoffs for significantly differential expressed genes. Before GSEA analysis, all Ensemble IDs of mouse genes were mapped to the corresponding human gene symbols. Subsequently, genes were ranked by $-\log_{10}(P \text{ value})$ and the sign of the $\log_2$(fold change). The ranks were then used for GSEA to determine genes sets that were enriched among the genes expressed in WT and B7-H3 KO samples (*72*). Gene sets or pathways in the KEGG, Hallmark, and GO databases with a false discovery rate of less than 0.05 were considered as statistically enriched.

Lentiviral plasmid construction

LentiCRISPRv2

CRISPRko sgRNA were designed using the Genetic Perturbation Platform Web Portal of the Broad Institute (https://portals.broadinstitute.org/gpp/public/analysis-tools/sgrna-design). The sequences of B7-H3 sgRNA were as follows: sgRNA1, 5′-CGCGTCCGAGTAACCGACGA-3′, targeting exon 3, and sgRNA 2, 5′-GTGTTCTGGAAGGATGGACA-3′,

targeting exon 4. The top two nontargeted control sgRNA sequences were selected from the Brie Library Control sgRNAs list (www.addgene.org/pooled-library/broadgpp-mouse-knockout-brie/): Scramble 1, 5′-AAAAAGTCCGCGATTACGTC-3′ and Scramble 2, 5′-AAAACGGCTCGATCGGTGAT-3′. Two oligonucleotides containing each sgRNA (primers #1 to #8) with 5′ overhang Bsbs I digestion sites were designed to clone the construct into the lentiCRISPR v2 plasmid backbone (gift from F. Zhang; Addgene, plasmid #52961; http://n2t.net/addgene:52961; RRID:Addgene_52961) (*73*). The cloning protocol was adapted from the ZhangLab lentiCRISPRv2 and lentiGuide oligo cloning protocol (https://media.addgene.org/data/plasmids/52/52961/52961-attachment_B3x-Twla0bkYD.pdf). The lentiCRISPRv2 plasmid was linearized by enzymatic digestion with Bbs I for 30 min at 37°C and purified using the QIAquick gel extraction kit. Each pair of oligonucleotides (100 mM) was annealed in T4 ligation buffer [New England Biolabs (NEB)] in a 10-µl reaction for 5 min at 95°C, followed by a ramp down to 25°C at 5°C/min. The ligation reaction was assembled in a volume of 11 µl as follow: 50 ng of linearized plasmid, 1 µl of oligo duplex diluted 1:200, 5 µl of 2X Quick Ligase Buffer (NEB), 1 µl of Quick Ligase (NEB), and H_2O, and incubated at RT for 10 min. Last, Stbl3 *Escherichia coli* were transformed and plated on LB plate containing ampicillin. Colonies were cultured overnight in liquid LB for plasmid isolation using the ZymoPURE II Plasmid Midiprep Kit and for sequence validation.

pHIV-zgreen

Full-length B7-H3 was cloned into the pHIV-Zsgreen plasmid (gift from B. Welm and Z. Werb; Addgene, plasmid #18121; http://n2t.net/addgene:18121; RRID:Addgene_18121) (*74*) using the NEB Gibson Assembly Cloning Kit, according to the manufacturer's instructions. Briefly, the pHIV-Zsgreen vector was linearized by sequential enzymatic digestion with Hpa I and Not I and purified using the QIAquick gel extraction kit. B7-H3 DNA insert was amplified from a B7-H3-MSCV plasmid by PCR using the Q5 High-Fidelity DNA Polymerase (NEB) and a forward primer with 5′ overhang Not I site (primer #9) and reverse primer with 5′ overhang Hpa I site (primer #10). The PCR-amplified insert was ligated to the linearized vector according to the Gibson Assembly Protocol (E5510). Last, NEB 5-alpha Competent *E. coli* cells were transformed and plated on LB plate containing ampicillin. Colonies were cultured overnight in liquid LB for plasmid isolation using the ZymoPURE II Plasmid Midiprep Kit and for sequence validation.

Lentivirus production

One day before transfection, 293 T cells were seeded on collagen-coated 10-cm cell culture dish in DMEM with L-glutamine, 10% FBS, and 1% pen/strep, at a density allowing for 80% confluency after 24 hours. Cells were transduced using a jetPRIME transfection reagent (Polyplus) according to the manufacturer's protocol. Briefly, the lentiviral vector containing the expression cassette was cotransfected with the envelope expressing plasmid pCI-VSVG (a gift from G. Nolan; Addgene, plasmid #1733; http://n2t.net/addgene:1733; RRID:Addgene_1733) and the lentiviral packaging plasmid pCMVR8.74 (gift from D. Trono; Addgene, plasmid #22036; http://n2t.net/addgene:22036; RRID:Addgene_22036) for 4 hours. Then, the transfection medium was replaced with fresh DMEM with L-glutamine, 10% FBS, and 1% pen/strep. Forty-eight hours later, the viral supernatant was collected, filtered through 0.45-µm mesh to remove cellular debris, and stored at −80°C.

Lentivirus transduction

For B7-H3 KO lines

One day before transduction, 2.7×10^5 Ing-svf cells were plated in a 10-cm cell culture dish. Cells were transduced overnight with 1 ml of viral supernatant in 10 ml of DMEM with L-glutamine, 10% FBS, and 1% pen/strep with polybrene (4 µg/ml). The medium was replaced with fresh medium containing puromycin (2 µg/ml). After 2 weeks of antibiotic selection, WT and B7-H3 KO Ing-svf cells were isolated by FACS and cultured as stable cell lines.

For B7-H3–overexpressing line

One day before transduction, 1×10^5 Ing-svf cells were plated in a 60-mm cell culture dish. Cells were transduced overnight with 1 ml of viral supernatant in 3 ml of DMEM with L-glutamine, 10% FBS, 1% pen/strep with polybrene (4 µg/ml). Two days later, transduction efficiency was assessed by B7-H3 FACS staining and GFP expression. One week after transduction, GFP^+ transduced cells were isolated by FACS with a BD FACSAria (Becton Dickinson) and subsequently cultured as stable GFP^+WT Ing-svf and $GFP^+B7\text{-}H3^{high}$ Ing-svf.

Cell proliferation assay

After magnetic isolation, APs were cultured ex vivo and passaged once. Equal number of cells was plated in triplicate in a flat-bottom 96-well plate. Two days later, 10 µl of the CCK-8 (Dojindo) solution was added to each well, and the plate was incubated for 3 hours at 37°C, 5% CO_2. The absorbance at 450 nm was measured using a microplate reader.

In vivo lipolysis

Weight-matched WT and B7-H3 KO mice were injected with isoproterenol (10 mg/kg) (Sigma-Aldrich) intraperitoneally at 5 weeks old. Blood was collected before and after the injection at 0, 10, 20, 30, and 60 min. Free glycerol was detected in the plasma by quantitative enzymatic reaction using the free glycerol reagent (Sigma-Aldrich, F6428) and glycerol standard (Sigma-Aldrich, G7793) and per the manufacturer's instructions.

Statistical analysis

Data were expressed as means ± SEM. The statistical test used in each quantification is reported in the figure legends. Differences were considered significant when the P value was less than 0.05 ($P < 0.05$). The GraphPad Prism statistical software program (GraphPad Software version 8) was used for all analyses.

SUPPLEMENTARY MATERIALS

Supplementary material for this article is available at https://science.org/doi/10.1126/sciadv.abm7012

View/request a protocol for this paper from *Bio-protocol*.

REFERENCES AND NOTES

1. M. Janakiram, U. A. Shah, W. Liu, A. Zhao, M. P. Schoenberg, X. Zang, The third group of the B7-CD28 immune checkpoint family: HHLA2, TMIGD2, B7x, and B7-H3. *Immunol. Rev.* **276**, 26–39 (2017).
2. E. Picarda, K. C. Ohaegbulam, X. Zang, Molecular pathways: Targeting B7-H3 (CD276) for human cancer immunotherapy. *Clin. Cancer Res.* **22**, 3425–3431 (2016).
3. S. Lim, H. Liu, L. M. da Silva, R. Arora, Z. Liu, J. B. Phillips, D. C. Schmitt, T. Vu, S. McClellan, Y. Lin, W. Lin, G. A. Piazza, O. Fodstad, M. Tan, Immunoregulatory protein B7-H3 reprograms glucose metabolism in cancer cells by ros-mediated stabilization of HIF1α. *Cancer Res.* **76**, 2231–2242 (2016).
4. T. Shi, Y. Ma, L. Cao, S. Zhan, Y. Xu, F. Fu, C. Liu, G. Zhang, Z. Wang, R. Wang, H. Lu, B. Lu, W. Chen, X. Zhang, B7-H3 promotes aerobic glycolysis and chemoresistance in colorectal cancer cells by regulating HK2. *Cell Death Dis.* **10**, 308 (2019).

5. C. Hales, M. Carroll, C. Fryar, C. Ogden, "Prevalence of obesity and severe obesity among adults: United States, 2017–2018," *NCHS Data Brief* (no. 360) (National Center for Health Statistics, 2020).
6. M. Asai, S. Ramachandrappa, M. Joachim, Y. Shen, R. Zhang, N. Nuthalapati, V. Ramanathan, D. E. Strochlic, P. Ferket, K. Linhart, C. Ho, T. V. Novoselova, S. Garg, M. Ridderstråle, C. Marcus, J. N. Hirschhorn, J. M. Keogh, S. O'Rahilly, L. F. Chan, A. J. Clark, I. S. Farooqi, J. A. Majzoub, Loss of function of the melanocortin 2 receptor accessory protein 2 is associated with mammalian obesity. *Science* **341**, 275–278 (2013).
7. J. Huo, Y. Ma, J. J. Liu, Y. S. Ho, S. Liu, L. Y. Soh, S. Chen, S. Xu, W. Han, A. Hong, S. C. Lim, K. P. Lam, Loss of Fas apoptosis inhibitory molecule leads to spontaneous obesity and hepatosteatosis. *Cell Death Dis.* **7**, e2091 (2016).
8. A. E. Locke, B. Kahali, S. I. Berndt, A. E. Justice, T. H. Pers, F. R. Day, C. Powell, S. Vedantam, M. L. Buchkovich, J. Yang, D. C. Croteau-Chonka, T. Esko, T. Fall, T. Ferreira, S. Gustafsson, Z. Kutalik, J. Luan, R. Mägi, J. C. Randall, T. W. Winkler, A. R. Wood, T. Workalemahu, J. D. Faul, J. A. Smith, J. H. Zhao, W. Zhao, J. Chen, R. Fehrmann, Å. K. Hedman, J. Karjalainen, E. M. Schmidt, D. Absher, N. Amin, D. Anderson, M. Beekman, J. L. Bolton, J. L. Bragg-Gresham, S. Buyske, A. Demirkan, G. Deng, G. B. Ehret, B. Feenstra, M. F. Feitosa, K. Fischer, A. Goel, J. Gong, A. U. Jackson, S. Kanoni, M. E. Kleber, K. Kristiansson, U. Lim, V. Lotay, M. Mangino, I. M. Leach, C. Medina-Gomez, S. E. Medland, M. A. Nalls, C. D. Palmer, D. Pasko, S. Pechlivanis, M. J. Peters, I. Prokopenko, D. Shungin, A. Stančáková, R. J. Strawbridge, Y. J. Sung, T. Tanaka, A. Teumer, S. Trompet, S. W. van der Laan, J. van Setten, J.a. V. Van Vliet-Ostaptchouk, Z. Wang, L. Yengo, W. Zhang, A. Isaacs, E. Albrecht, J. Ärnlöv, G. M. Arscott, A. P. Attwood, S. Bandinelli, A. Barrett, I. N. Bas, C. Bellis, A. J. Bennett, C. Berne, R. Blagieva, M. Blüher, S. Böhringer, L. L. Bonnycastle, Y. Böttcher, H. A. Boyd, M. Bruinenberg, I. H. Caspersen, Y.-D. I. Chen, R. Clarke, E. W. Daw, A. J. M. de Craen, G. Delgado, M. Dimitriou, A. S. F. Doney, N. Eklund, K. Estrada, E. Eury, L. Folkersen, R. M. Fraser, M. E. Garcia, F. Geller, V. Giedraitis, B. Gigante, A. S. Go, A. Golay, A. H. Goodall, S. D. Gordon, M. Gorski, H.-J. Grabe, H. Grallert, T. B. Grammer, J. Gräßler, H. Grönberg, C. J. Groves, G. Gusto, J. Haessler, P. Hall, T. Haller, G. Hallmans, C. A. Hartman, M. Hassinen, C. Hayward, N. L. Heard-Costa, Q. Helmer, C. Hengstenberg, O. Holmen, J.-J. Hottenga, A. L. James, J. M. Jeff, Å. Johansson, J. Jolley, T. Juliusdottir, L. Kinnunen, W. Koenig, M. Koskenvuo, W. Kratzer, J. Laitinen, C. Lamina, K. Leander, N. R. Lee, P. Lichtner, L. Lind, J. Lindström, K. S. Lo, S. Lobbens, R. Lorbeer, Y. Lu, F. Mach, P. K. E. Magnusson, A. Mahajan, W.e. L. Mc Ardle, S. M. Lachlan, C. Menni, S. Merger, E. Mihailov, L. Milani, A. Moayyeri, K. L. Monda, M. A. Morken, A. Mulas, G. Müller, M. Müller-Nurasyid, A. W. Musk, R. Nagaraja, M. M. Nöthen, I. M. Nolte, S. Pilz, N. W. Rayner, F. Renstrom, R. Rettig, J. S. Ried, S. Ripke, N. R. Robertson, L. M. Rose, S. Sanna, H. Scharnagl, S. Scholtens, F. R. Schumacher, W. R. Scott, T. Seufferlein, J. Shi, A. V. Smith, J. Smolonska, A. V. Stanton, V. Steinthorsdottir, K. Stirrups, H. M. Stringham, J. Sundström, M. A. Swertz, A. J. Swift, A.-C. Syvänen, S.-T. Tan, B. O. Tayo, B. Thorand, G. Thorleifsson, J. P. Tyrer, H.-W. Uh, L. Vandenput, F. C. Verhulst, S. H. Vermeulen, N. Verweij, J. M. Vonk, L. L. Waite, H. R. Warren, D. Waterworth, M. N. Weedon, L. R. Wilkens, C. Willenborg, T. Wilsgaard, M. K. Wojczynski, A. Wong, A. F. Wright, Q. Zhang; The Life Lines Cohort Study, E. P. Brennan, M. Choi, Z. Dastani, A. W. Drong, P. Eriksson, A. Franco-Cereceda, J. R. Gådin, A. G. Gharavi, M. E. Goddard, R. E. Handsaker, J. Huang, F. Karpe, S. Kathiresan, S. Keildson, K. Kiryluk, M. Kubo, J.-Y. Lee, L. Liang, R. P. Lifton, B. Ma, S. A. McCarroll, A. J. Mc Knight, J. L. Min, M. F. Moffatt, G. W. Montgomery, J. M. Murabito, G. Nicholson, D. R. Nyholt, Y. Okada, J. R. B. Perry, R. Dorajoo, E. Reinmaa, R. M. Salem, N. Sandholm, R. A. Scott, L. Stolk, A. Takahashi, T. Tanaka, F. M. van't Hooft, A. A. E. Vinkhuyzen, H.-J. Westra, W. Zheng, K. T. Zondervan; ADIPOGen Consortium; AGEN-BMI Working Group; CARDIOGRAMplusC4D Consortium; CKDGen Consortium; GLGC; ICBP; MAGIC Investigators; MuTHER Consortium; MIGen Consortium; PAGE Consortium; ReproGen Consortium; GENIE Consortium; International Endogene Consortium, A. C. Heath, D. Arveiler, S. J. L. Bakker, J. Beilby, R. N. Bergman, J. Blangero, P. Bovet, H. Campbell, M. J. Caulfield, G. Cesana, A. Chakravarti, D. I. Chasman, P. S. Chines, F. S. Collins, D. C. Crawford, L. A. Cupples, D. Cusi, J. Danesh, U. de Faire, H. M. den Ruijter, A. F. Dominiczak, R. Erbel, J. Erdmann, J. G. Eriksson, M. Farrall, S. B. Felix, E. Ferrannini, J. Ferrières, I. Ford, N. G. Forouhi, T. Forrester, O. H. Franco, R. T. Gansevoort, P. V. Gejman, C. Gieger, O. Gottesman, V. Gudnason, U. Gyllensten, A. S. Hall, T. B. Harris, A. T. Hattersley, A. A. Hicks, L. A. Hindorff, A. D. Hingorani, A. Hofman, G. Homuth, G. K.e. Hovingh, S. E. Humphries, S. C. Hunt, E. Hyppönen, T. Illig, K. B. Jacobs, M.-R. Jarvelin, K.-H. Jöckel, B. Johansen, P. Jousilahti, J. W. Jukema, A. M. Jula, J. Kaprio, J. J. P. Kastelein, S. M. Keinanen-Kiukaanniemi, L. A. Kiemeney, P. Knekt, J. S. Kooner, C. Kooperberg, P. Kovacs, A. T. Kraja, M. Kumari, J. Kuusisto, T. A. Lakka, C. Langenberg, L. L. Marchand, T. Lehtimäki, V. Lyssenko, S. Männistö, A. Marette, T. C. Matise, C.o. A. Mc Kenzie, B. M. Knight, F. L. Moll, A. D. Morris, A. P. Morris, J. C. Murray, M. Nelis, C. Ohlsson, A. J. Oldehinkel, K. K. Ong, P. A. F. Madden, G. Pasterkamp, J. F. Peden, A. Peters, D. S. Postma, P. P. Pramstaller, J. F. Price, L. Qi, O. T. Raitakari, T. Rankinen, D. C. Rao, T. K. Rice, P. M. Ridker, J. D. Rioux, M. D. Ritchie, I. Rudan, V. Salomaa, N. J. Samani, J. Saramies, M. A. Sarzynski, H. Schunkert, P. E. H. Schwarz, P. Sever, A. R. Shuldiner, J. Sinisalo, R. P. Stolk, K. Strauch, A. Tönjes, D.-A. Trégouët, A. Tremblay, E. Tremoli, J. Virtamo, M.-C. Vohl, U. Völker, G. Waeber, G. Willemsen, J. C. Witteman, M. C.a. Zillikens, L. S. Adair, P. Amouyel, F. W. Asselbergs, T. L. Assimes, M. Bochud, B. O. Boehm, E. Boerwinkle, S. R. Bornstein, E. P. Bottinger, C. Bouchard, S. Cauchi, J. C. Chambers, S. J. Chanock, R. S. Cooper, P.a. I. W. de Bakker, G. Dedoussis, L. Ferrucci, P. W. Franks, P. Froguel, L. C. Groop, C. A. Haiman, A. Hamsten, J. Hui, D. J. Hunter, K. Hveem, R. C. Kaplan, M. Kivimaki, D. Kuh, M. Laakso, Y. Liu, N. G. Martin, W. März, M. Melbye, A. Metspalu, S. Moebus, P. B. Munroe, I. Njølstad, B. A. Oostra, C. N. A. Palmer, N. L. Pedersen, M. Perola, L. Pérusse, U. Peters, C. Power, T. Quertermous, R. Rauramaa, F. Rivadeneira, T. E. Saaristo, D. Saleheen, N. Sattar, E. E. Schadt, D. Schlessinger, P. E.I. Slagboom, H. Snieder, T. D. Spector, U. Thorsteinsdottir, M. Stumvoll, J. Tuomilehto, A. G. Uitterlinden, M. Uusitupa, P. van der Harst, M. Walker, H. Wallaschofski, N. J. Wareham, H. Watkins, D. R. Weir, H.-E. Wichmann, J. F. Wilson, P. Zanen, I. B. Borecki, P. Deloukas, C. S. Fox, I. M. Heid, J. R. O'Connell, D. P. Strachan, K. Stefansson, C. M. van Duijn, G. R. Abecasis, L. Franke, T. M. Frayling, M. I. McCarthy, P. M. Visscher, A. Scherag, C. J. Willer, M. Boehnke, K. L. Mohlke, C. M. Lindgren, J. S. Beckmann, I. Barroso, K. E. North, E. Ingelsson, J. N. Hirschhorn, R. J. F. Loos, E. K. Speliotes, Genetic studies of body mass index yield new insights for obesity biology. *Nature* **518**, 197–206 (2015).
9. D. N. Lorenzo, V. Bennett, Cell-autonomous adiposity through increased cell surface GLUT4 due to ankyrin-B deficiency. *Proc. Natl. Acad. Sci. U.S.A.* **114**, 12743–12748 (2017).
10. M. Civelek, Y. Wu, C. Pan, C. K. Raulerson, A. Ko, A. He, C. Tilford, N. K. Saleem, A. Stančáková, L. J. Scott, C. Fuchsberger, H. M. Stringham, A. U. Jackson, N. Narisu, P. S. Chines, K. S. Small, J. Kuusisto, B. W. Parks, P. Pajukanta, T. Kirchgessner, F. S. Collins, P. S. Gargalovic, M. Boehnke, M. Laakso, K. L. Mohlke, A. J. Lusis, Genetic regulation of adipose gene expression and cardio-metabolic traits. *Am. J. Hum. Genet.* **100**, 428–443 (2017).
11. E. Arner, N. Mejhert, A. Kulyté, P. J. Balwierz, M. Pachkov, M. Cormont, S. Lorente-Cebrián, A. Ehrlund, J. Laurencikiene, P. Hedén, K. Dahlman-Wright, J. F. Tanti, Y. Hayashizaki, M. Rydén, I. Dahlman, E. van Nimwegen, C. O. Daub, P. Arner, Adipose tissue microRNAs as regulators of CCL2 production in human obesity. *Diabetes* **61**, 1986–1993 (2012).
12. P. Petrus, N. Mejhert, P. Corrales, S. Lecoutre, Q. Li, E. Maldonado, A. Kulyté, Y. Lopez, M. Campbell, J. R. Acosta, J. Laurencikiene, I. Douagi, H. Gao, C. Martínez-Álvarez, P. Hedén, K. L. Spalding, A. Vidal-Puig, G. Medina-Gomez, P. Arner, M. Rydén, Transforming growth factor-beta3 regulates adipocyte number in subcutaneous white adipose tissue. *Cell Rep.* **25**, 551–560.e5 (2018).
13. I. P. Fischer, M. Irmler, C. W. Meyer, S. J. Sachs, F. Neff, M. Hrabě de Angelis, J. Beckers, M. H. Tschöp, S. M. Hofmann, S. Ussar, A history of obesity leaves an inflammatory fingerprint in liver and adipose tissue. *Int. J. Obes.* **42**, 507–517 (2018).
14. J. A. Dykstra, T. Facile, R. J. Patrick, K. R. Francis, S. Milanovich, J. M. Weimer, D. J. Kota, Concise review: Fat and furious: Harnessing the full potential of adipose-derived stromal vascular fraction. *Stem Cells Transl. Med.* **6**, 1096–1108 (2017).
15. S. Gesta, M. Blüher, Y. Yamamoto, A. W. Norris, J. Berndt, S. Kralisch, J. Boucher, C. Lewis, C. R. Kahn, Evidence for a role of developmental genes in the origin of obesity and body fat distribution. *Proc. Natl. Acad. Sci. U.S.A.* **103**, 6676–6681 (2006).
16. R. Berry, M. S. Rodeheffer, Characterization of the adipocyte cellular lineage in vivo. *Nat. Cell Biol.* **15**, 302–308 (2013).
17. A. Ehrlund, J. R. Acosta, C. Björk, P. Hedén, I. Douagi, P. Arner, J. Laurencikiene, The cell-type specific transcriptome in human adipose tissue and influence of obesity on adipocyte progenitors. *Sci. Data* **4**, 170164 (2017).
18. W. Sun, H. Dong, M. Balaz, M. Slyper, E. Drokhlyansky, G. Colleluori, A. Giordano, Z. Kovanicova, P. Stefanicka, L. Balazova, L. Ding, A. S. Husted, G. Rudofsky, J. Ukropec, S. Cinti, T. W. Schwartz, A. Regev, C. Wolfrum, snRNA-seq reveals a subpopulation of adipocytes that regulates thermogenesis. *Nature* **587**, 98–102 (2020).
19. K. Birsoy, R. Berry, T. Wang, O. Ceyhan, S. Tavazoie, J. M. Friedman, M. S. Rodeheffer, Analysis of gene networks in white adipose tissue development reveals a role for ETS2 in adipogenesis. *Development* **138**, 4709–4719 (2011).
20. Y. Wang, H. S. Sul, Pref-1 regulates mesenchymal cell commitment and differentiation through Sox9. *Cell Metab.* **9**, 287–302 (2009).
21. L. Satish, J. M. Krill-Burger, P. H. Gallo, S. D. Etages, F. Liu, B. J. Philips, S. Ravuri, K. G. Marra, W. A. LaFramboise, S. Kathju, J. P. Rubin, Expression analysis of human adipose-derived stem cells during in vitro differentiation to an adipocyte lineage. *BMC Med. Genet.* **8**, 41 (2015).
22. R. A. Saxton, D. M. Sabatini, mTOR signaling in growth, metabolism, and disease. *Cell* **169**, 361–371 (2017).
23. P. A. Carroll, B. W. Freie, H. Mathsyaraja, R. N. Eisenman, The MYC transcription factor network: Balancing metabolism, proliferation and oncogenesis. *Front. Med.* **12**, 412–425 (2018).
24. D. Rotter, H. Peiris, D. B. Grinsfelder, A. M. Martin, J. Burchfield, V. Parra, C. Hull, C. R. Morales, C. F. Jessup, D. Matusica, B. W. Parks, A. J. Lusis, N. U. N. Nguyen, M. Oh, I. Iyoke, T. Jakkampudi, D. R. McMillan, H. A. Sadek, M. J. Watt, R. K. Gupta, M. A. Pritchard,

D. J. Keating, B. A. Rothermel, Regulator of Calcineurin 1 helps coordinate whole-body metabolism and thermogenesis. *EMBO Rep.* **19**, e44706 (2018).
25. Y. R. Yu, H. Imrichova, H. Wang, T. Chao, Z. Xiao, M. Gao, M. Rincon-Restrepo, F. Franco, R. Genolet, W. C. Cheng, C. Jandus, G. Coukos, Y. F. Jiang, J. W. Locasale, A. Zippelius, P. S. Liu, L. Tang, C. Bock, N. Vannini, P. C. Ho, Disturbed mitochondrial dynamics in CD8(+) TILs reinforce T cell exhaustion. *Nat. Immunol.* **21**, 1540–1551 (2020).
26. K. Ito, T. Suda, Metabolic requirements for the maintenance of self-renewing stem cells. *Nat. Rev. Mol. Cell Biol.* **15**, 243–256 (2014).
27. A. Wanet, T. Arnould, M. Najimi, P. Renard, Connecting mitochondria, metabolism, and stem cell fate. *Stem Cells Dev.* **24**, 1957–1971 (2015).
28. D. L. Drehmer, A. M. de Aguiar, A. P. Brandt, L. Petiz, S. M. S. C. Cadena, C. K. Rebelatto, P. R. S. Brofman, F. Filipak Neto, B. Dallagiovanna, A. P. R. Abud, Metabolic switches during the first steps of adipogenic stem cells differentiation. *Stem Cell Res.* **17**, 413–421 (2016).
29. S. Heinonen, R. Jokinen, A. Rissanen, K. H. Pietilainen, White adipose tissue mitochondrial metabolism in health and in obesity. *Obes. Rev.* **21**, e12958 (2020).
30. J. R. Ingram, M. Dougan, M. Rashidian, M. Knoll, E. J. Keliher, S. Garrett, S. Garforth, O. S. Blomberg, C. Espinosa, A. Bhan, S. C. Almo, R. Weissleder, H. Lodish, S. K. Dougan, H. L. Ploegh, PD-L1 is an activation-independent marker of brown adipocytes. *Nat. Commun.* **8**, 647 (2017).
31. S. M. Harakeh, I. Khan, T. Kumosani, E. Barbour, S. B. Almasaudi, S. M. Bahijri, S. M. Alfadul, G. M. A. Ajabnoor, E. I. Azhar, Gut microbiota: A contributing factor to obesity. *Front. Cell. Infect. Microbiol.* **6**, 95 (2016).
32. C. Petersen, R. Bell, K. A. Klag, S. H. Lee, R. Soto, A. Ghazaryan, K. Buhrke, H. A. Ekiz, K. S. Ost, S. Boudina, R. M. O'Connell, J. E. Cox, C. J. Villanueva, W. Z. Stephens, J. L. Round, T cell-mediated regulation of the microbiota protects against obesity. *Science* **365**, eaat9351 (2019).
33. M. Vijay-Kumar, J. D. Aitken, F. A. Carvalho, T. C. Cullender, S. Mwangi, S. Srinivasan, S. V. Sitaraman, R. Knight, R. E. Ley, A. T. Gewirtz, Metabolic syndrome and altered gut microbiota in mice lacking Toll-like receptor 5. *Science* **328**, 228–231 (2010).
34. H. Du, K. Hirabayashi, S. Ahn, N. P. Kren, S. A. Montgomery, X. Wang, K. Tiruthani, B. Mirlekar, D. Michaud, K. Greene, S. G. Herrera, Y. Xu, C. Sun, Y. Chen, X. Ma, C. R. Ferrone, Y. Pylayeva-Gupta, J. J. Yeh, R. Liu, B. Savoldo, S. Ferrone, G. Dotti, Antitumor responses in the absence of toxicity in solid tumors by targeting B7-H3 via chimeric antigen receptor T cells. *Cancer Cell* **35**, 221–237.e8 (2019).
35. K. A. Hofmeyer, A. Ray, X. Zang, The contrasting role of B7-H3. *Proc. Natl. Acad. Sci. U.S.A.* **105**, 10277–10278 (2008).
36. J. Leitner, C. Klauser, W. F. Pickl, J. Stöckl, O. Majdic, A. F. Bardet, D. P. Kreil, C. Dong, T. Yamazaki, G. Zlabinger, K. Pfistershammer, P. Steinberger, B7-H3 is a potent inhibitor of human T-cell activation: No evidence for B7-H3 and TREML2 interaction. *Eur. J. Immunol.* **39**, 1754–1764 (2009).
37. V. Vigdorovich, U. A. Ramagopal, E. Lázár-Molnár, E. Sylvestre, J. S. Lee, K. A. Hofmeyer, X. Zang, S. G. Nathenson, S. C. Almo, Structure and T cell inhibition properties of B7 family member, B7-H3. *Structure* **21**, 707–717 (2013).
38. D. Luo, H. Xiao, J. Dong, Y. Li, G. Feng, M. Cui, S. Fan, B7-H3 regulates lipid metabolism of lung cancer through SREBP1-mediated expression of FASN. *Biochem. Biophys. Res. Commun.* **482**, 1246–1251 (2017).
39. S. Ussar, K. Y. Lee, S. N. Dankel, J. Boucher, M.-F. Haering, A. Kleinridders, T. Thomou, R. Xue, Y. Macotela, A. M. Cypess, Y.-H. Tseng, G. Mellgren, C. R. Kahn, ASC-1, PAT2, and P2RX5 are cell surface markers for white, beige, and brown adipocytes. *Sci. Transl. Med.* **6**, 247ra103 (2014).
40. J. H. Stern, J. M. Rutkowski, P. E. Scherer, Adiponectin, leptin, and fatty acids in the maintenance of metabolic homeostasis through adipose tissue crosstalk. *Cell Metab.* **23**, 770–784 (2016).
41. M. Maffei, J. Halaas, E. Ravussin, R. E. Pratley, G. H. Lee, Y. Zhang, H. Fei, S. Kim, R. Lallone, S. Ranganathan, P. A. Kern, J. M. Friedman, Leptin levels in human and rodent: Measurement of plasma leptin and ob RNA in obese and weight-reduced subjects. *Nat. Med.* **1**, 1155–1161 (1995).
42. F. J. Ortega, D. Mayas, J. M. Moreno-Navarrete, V. Catalán, J. Gómez-Ambrosi, E. Esteve, J. I. Rodriguez-Hermosa, B. Ruiz, W. Ricart, B. Peral, G. Fruhbeck, F. J. Tinahones, J. M. Fernández-Real, The gene expression of the main lipogenic enzymes is downregulated in visceral adipose tissue of obese subjects. *Obesity (Silver Spring)* **18**, 13–20 (2010).
43. J. Lu, J. Zhao, H. Meng, X. Zhang, Adipose tissue-resident immune cells in obesity and type 2 diabetes. *Front. Immunol.* **10**, 1173 (2019).
44. S. Talukdar, D. Y. Oh, G. Bandyopadhyay, D. Li, J. Xu, J. McNelis, M. Lu, P. Li, Q. Yan, Y. Zhu, J. Ofrecio, M. Lin, M. B. Brenner, J. M. Olefsky, Neutrophils mediate insulin resistance in mice fed a high-fat diet through secreted elastase. *Nat. Med.* **18**, 1407–1412 (2012).
45. J. R. Brestoff, D. Artis, Immune regulation of metabolic homeostasis in health and disease. *Cell* **161**, 146–160 (2015).
46. L. Russo, C. N. Lumeng, Properties and functions of adipose tissue macrophages in obesity. *Immunology* **155**, 407–417 (2018).
47. A. H. Sharpe, Introduction to checkpoint inhibitors and cancer immunotherapy. *Immunol. Rev.* **276**, 5–8 (2017).
48. S. Lim, J. B. Phillips, L. Madeira da Silva, M. Zhou, O. Fodstad, L. B. Owen, M. Tan, Interplay between immune checkpoint proteins and cellular metabolism. *Cancer Res.* **77**, 1245–1249 (2017).
49. C. H. Chang, J. Qiu, D. O'Sullivan, M. D. Buck, T. Noguchi, J. D. Curtis, Q. Chen, M. Gindin, M. M. Gubin, G. J. W. van der Windt, E. Tonc, R. D. Schreiber, E. J. Pearce, E. L. Pearce, Metabolic competition in the tumor microenvironment is a driver of cancer progression. *Cell* **162**, 1229–1241 (2015).
50. J. Zuo, B. Wang, M. Long, Z. Gao, Z. Zhang, H. Wang, X. Wang, R. Li, K. Dong, H. Zhang, The type 1 transmembrane glycoprotein B7-H3 interacts with the glycolytic enzyme ENO1 to promote malignancy and glycolysis in HeLa cells. *FEBS Lett.* **592**, 2476–2488 (2018).
51. A. M. Intlekofer, L. W. S. Finley, Metabolic signatures of cancer cells and stem cells. *Nat. Metab.* **1**, 177–188 (2019).
52. W. K. Suh, S. X. Wang, A. H. Jheon, L. Moreno, S. K. Yoshinaga, B. Ganss, J. Sodek, M. D. Grynpas, T. W. Mak, The immune regulatory protein B7-H3 promotes osteoblast differentiation and bone mineralization. *Proc. Natl. Acad. Sci. U.S.A.* **101**, 12969–12973 (2004).
53. A. R. Guntur, A. A. Gerencser, P. T. le, V. E. DeMambro, S. A. Bornstein, S. A. Mookerjee, D. E. Maridas, D. E. Clemmons, M. D. Brand, C. J. Rosen, Osteoblast-like MC3T3-E1 cells prefer glycolysis for ATP production but adipocyte-like 3T3-L1 cells prefer oxidative phosphorylation. *J. Bone Miner. Res.* **33**, 1052–1065 (2018).
54. A. K. Picke, G. M. Campbell, M. Blüher, U. Krügel, F. N. Schmidt, E. Tsourdi, M. Winzer, M. Rauner, V. Vukicevic, B. Busse, J. Salbach-Hirsch, J. P. Tuckermann, J. C. Simon, U. Anderegg, L. C. Hofbauer, A. Saalbach, Thy-1 (CD90) promotes bone formation and protects against obesity. *Sci. Transl. Med.* **10**, eaao6806 (2018).
55. J. Zhang, J. Wang, D. M. Marzese, X. Wang, Z. Yang, C. Li, H. Zhang, J. Zhang, C. C. Chen, D. F. Kelly, W. Hua, D. S. B. Hoon, Y. Mao, B7H3 regulates differentiation and serves as a potential biomarker and theranostic target for human glioblastoma. *Lab. Investig.* **99**, 1117–1129 (2019).
56. Y. Son, S. M. Kwon, J. Y. Cho, CD276 (B7-H3) maintains proliferation and regulates differentiation in angiogenic function in late endothelial progenitor cells. *Stem Cells* **37**, 382–394 (2019).
57. A. Raajendiran, G. Ooi, J. Bayliss, P. E. O'Brien, R. B. Schittenhelm, A. K. Clark, R. A. Taylor, M. S. Rodeheffer, P. R. Burton, M. J. Watt, Identification of metabolically distinct adipocyte progenitor cells in human adipose tissues. *Cell Rep.* **27**, 1528–1540.e7 (2019).
58. A. Carrière, D. Lagarde, Y. Jeanson, J.-C. Portais, A. Galinier, I. Ader, L. Casteilla, The emerging roles of lactate as a redox substrate and signaling molecule in adipose tissues. *J. Physiol. Biochem.* **76**, 241–250 (2020).
59. L. L. Lehrskov, R. H. Christensen, The role of interleukin-6 in glucose homeostasis and lipid metabolism. *Semin. Immunopathol.* **41**, 491–499 (2019).
60. V. Wallenius, K. Wallenius, B. Ahrén, M. Rudling, H. Carlsten, S. L. Dickson, C. Ohlsson, J. O. Jansson, Interleukin-6-deficient mice develop mature-onset obesity. *Nat. Med.* **8**, 75–79 (2002).
61. E. W. Petersen, A. L. Carey, M. Sacchetti, G. R. Steinberg, S. L. Macaulay, M. A. Febbraio, B. K. Pedersen, Acute IL-6 treatment increases fatty acid turnover in elderly humans in vivo and in tissue culture in vitro. *Am. J. Physiol. Endocrinol. Metab.* **288**, E155–E162 (2005).
62. T. D. Muller, M. Bluher, M. H. Tschop, R. D. DiMarchi, Anti-obesity drug discovery: Advances and challenges. *Nat. Rev. Drug Discov.* **21**, 201–223 (2022).
63. D. V. R. Prasad, T. Nguyen, Z. Li, Y. Yang, J. Duong, Y. Wang, C. Dong, Murine B7-H3 is a negative regulator of T cells. *J. Immunol.* **173**, 2500–2506 (2004).
64. Z. Liu, W. Zhang, J. B. Phillips, R. Arora, S. McClellan, J. Li, J. H. Kim, R. W. Sobol, M. Tan, Immunoregulatory protein B7-H3 regulates cancer stem cell enrichment and drug resistance through MVP-mediated MEK activation. *Oncogene* **38**, 88–102 (2019).
65. J. Ben, B. Jiang, D. Wang, Q. Liu, Y. Zhang, Y. Qi, X. Tong, L. Chen, X. Liu, Y. Zhang, X. Zhu, X. Li, H. Zhang, H. Bai, Q. Yang, J. Ma, E. A. C. Wiemer, Y. Xu, Q. Chen, Major vault protein suppresses obesity and atherosclerosis through inhibiting IKK–NF-κB signaling mediated inflammation. *Nat. Commun.* **10**, 1801 (2019).
66. W. K. Suh, B. U. Gajewska, H. Okada, M. A. Gronski, E. M. Bertram, W. Dawicki, G. S. Duncan, J. Bukczynski, S. Plyte, A. Elia, A. Wakeham, A. Itie, S. Chung, J. da Costa, S. Arya, T. Horan, P. Campbell, K. Gaida, P. S. Ohashi, T. H. Watts, S. K. Yoshinaga, M. R. Bray, M. Jordana, T. W. Mak, The B7 family member B7-H3 preferentially down-regulates T helper type 1-mediated immune responses. *Nat. Immunol.* **4**, 899–906 (2003).
67. L. Scandiuzzi, K. Ghosh, K. A. Hofmeyer, Y. M. Abadi, E. Lázár-Molnár, E. Y. Lin, Q. Liu, H. Jeon, S. C. Almo, L. Chen, S. G. Nathenson, X. Zang, Tissue-expressed B7-H1 critically controls intestinal inflammation. *Cell Rep.* **6**, 625–632 (2014).
68. A. I. Mina, R. A. Le Clair, K. B. Le Clair, D. E. Cohen, L. Lantier, A. S. Banks, CalR: A web-based analysis tool for indirect calorimetry experiments. *Cell Metab.* **28**, 656–666.e1 (2018).
69. N. Martinez-Lopez, M. Garcia-Macia, S. Sahu, D. Athonvarangkul, E. Liebling, P. Merlo, F. Cecconi, G. J. Schwartz, R. Singh, Autophagy in the CNS and periphery coordinate

lipophagy and lipolysis in the brown adipose tissue and liver. *Cell Metab.* **23**, 113–127 (2016).
70. A. Dobin, T. R. Gingeras, Mapping RNA-seq reads with STAR. *Curr. Protoc. Bioinformatics* **51**, 11.14.11–11.14.19 (2015).
71. M. D. Robinson, D. J. McCarthy, G. K. Smyth, edgeR: A Bioconductor package for differential expression analysis of digital gene expression data. *Bioinformatics* **26**, 139–140 (2010).
72. A. Subramanian, P. Tamayo, V. K. Mootha, S. Mukherjee, B. L. Ebert, M. A. Gillette, A. Paulovich, S. L. Pomeroy, T. R. Golub, E. S. Lander, J. P. Mesirov, Gene set enrichment analysis: A knowledge-based approach for interpreting genome-wide expression profiles. *Proc. Natl. Acad. Sci. U.S.A.* **102**, 15545–15550 (2005).
73. N. E. Sanjana, O. Shalem, F. Zhang, Improved vectors and genome-wide libraries for CRISPR screening. *Nat. Methods* **11**, 783–784 (2014).
74. B. E. Welm, G. J. Dijkgraaf, A. S. Bledau, A. L. Welm, Z. Werb, Lentiviral transduction of mammary stem cells for analysis of gene function during development and cancer. *Cell Stem Cell* **2**, 90–102 (2008).

Acknowledgments: We thank K. Hofmeyer, L. Scandiuzzi, and J. Chinai for breeding mice and early work; E. Tarabra and M. Aoun for technical assistance with tissue respirometry; R. Gupta for providing Ing-svf cells; and A. Briceno for technical assistance on the Leica SP8 confocal microscope; and the Flow Cytometry Core Facility and Analytical Imaging Facility.

Funding: the Flow Cytometry Core Facility and Analytical Imaging Facility is partially supported through NCI Cancer Center Support grant P30CA013330. This work used a high-speed/resolution P250 whole slide scanner and the Leica SP8 confocal microscope that were purchased with funding from National Institutes of Health SIG grants 1S10OD019961-01 and 1S10OD023591-01, respectively. E.B. is supported by ERC grant StG #804418, the Wallenberg Centre for Molecular and Translational Medicine at University of Gothenburg and Knut and Alice Wallenberg Foundation, the Swedish Research Council (#2016/82), and SSMF (#S150086). This study was supported by National Institutes of Health grants R01DK100525 (X.Z.) and P30DK020541 (Einstein-Mount Sinai Diabetes Research Center). **Author contributions:** Conceptualization: E.P., R.S., J.P., and X.Z. Formal analysis: P.M.G.J. and D.Z. Investigation: E.P., H.Z., and M.R.R. Resources: E.B. and V.W. Writing—Original draft: E.P. Writing—Review and editing: E.P., P.M.G.J., H.Z., M.R.R., D.Z., E.B., R.S., J.P., and X.Z. Visualization: E.P. Funding acquisition and supervision: X.Z. **Competing interests:** The authors declare that they have no competing interests. **Data and materials availability:** All data needed to evaluate the conclusions in the paper are present in the paper and/or the Supplementary Materials.

Submitted 5 October 2021
Accepted 11 March 2022
Published 27 April 2022
10.1126/sciadv.abm7012